Towards a new implementation of 'MREOM-CC', with application to MO^+ dimers (M = V, Cr, Mn, Fe, Co, Ni)

by

Johnathan Peter Steffen

A thesis

presented to the University of Waterloo

in fulfillment of the

thesis requirement for the degree of

Master of Science

in

Chemistry

Waterloo, Ontario, Canada, 2018

Author's Declaration

I hereby declare that I am the sole author of this thesis. This is a true copy of the thesis, including any required final revisions, as accepted by my examiners.

I understand that my thesis may be made electronically available to the public.

Abstract

Multi Reference Equation of Motion Coupled Cluster (MREOM-CC) is an electronic structure method that allows the calculation of many electronic states simultaneously. A sequence of transformations are applied to a Hamiltonian allowing for a subsequent diagonalization of a much smaller subspace. These transformations preserve the eigenvalues of the original Hamiltonian, and paradoxically calculations increase in accuracy while simultaneously reducing the cost of the calculation. MREOM has previously been used to calculate transition metal atom spectra as well as vertical excitation spectra from organic molecules and transition metal complexes.

In this thesis, MREOM is used to calculate a potential energy surface for several systems containing many excited states. The systems studied in this thesis are positively charged diatomic transition metal oxides (MO^+, M = V, Cr, Mn, Fe, Co, Ni) chosen for both their electronic complexity as well as the opportunity for a tandem experimental study in the Hopkins lab. Calculations were approached using either a high spin or low spin regime for the reference states of each system. High spin systems converged at high interatomic distance, but generally exhibited discontinuities. Low spin systems appeared smooth, but were troublesome to set up. However, MREOM is not recommended for complicated potential energy surfaces until further improvements can be made.

In a second project an improved algorithm is developed for the time-consuming final diagonalization step in MREOM. Using a carefully designed data structure for multiple electronic states the critical multiplication of "$G \cdot C$" is carried out efficiently, with minimal resorting and optimized using the Basic Linear Algebra Subroutines (BLAS) library. The implementation is not yet complete, and requires interfacing with the rest of the code.

Acknowledgements

Firstly, thank you so much to my two supervisors Scott and Marcel, who gave me this amazing opportunity and helped me grow so much along the way. I appreciate the constant support and advice, academic or not. Also, thanks for the chairs and table, Scott! I'd also like to thank the innumerable amazing group members I've had the pleasure to work with, especially Pat, Steve and Mike, for their constant moral support and for being awesome friends. Lastly, thank you to my Mom and Dad for believing in me all this time. I couldn't have done it without any of you. Thank you all so much!

Table of Contents

Author's Declaration ... ii
Abstract ... iii
Acknowledgements ... iv
Table of Contents ... v
List of Figures ... vii
List of Tables ... viii
List of abbreviations ... ix
Chapter 1: Introduction to Electronic Structure Theory ... 1
Chapter 2: Multi-Reference Equation of Motion Coupled Cluster Theory ... 4
Chapter 3: Multi-Reference Equation-Of-Motion Study of MO+ ... 13
3.1: Systems in Study: Transition Metal Oxide Cations ... 14
3.2: Calculation Strategy: 'High spin' and 'Low spin' ... 17
3.3: Basics of Complete Active Space Calculations ... 19
3.4: CASSCF Calculation Results and Discussion ... 24
3.5: Basics of Multi Reference Equation of Motion Calculations ... 27
3.6: MREOM Calculation Results and Discussion ... 30
3.6.1: MnO^+ Calculation and Discussion ... 32
3.6.2: FeO^+ Calculation and Discussion ... 38
3.6.3: CoO^+ Calculation and Discussion ... 39
3.6.4 NiO^+ Calculation and Discussion ... 41
3.6.5 CrO^+ Calculation and Discussion ... 43
3.6.6 VO^+ Calculation and Discussion ... 45
3.7: Conclusion ... 47
Chapter 4: New Method for Implementing MREOM ... **5**50
4.1 Code example of one body Hamiltonian ... 57
4.2 Accounting for Spin Cases ... 62
4.3 Code Example of two body Hamiltonian ... 64
4.4 Future Work Implementing the New Algorithm ... 70
Chapter 5 ... 72
Conclusion and Future Direction ... 72
References ... 75
Appendix A: List of Contributions to Hamiltonian in CI Code ... 77
Appendix B: Complete Active Space Orbital Occupancies ... 80

High Spin CAS Orbital Occupancies 80
Low Spin CAS Orbital Occupancies 84
Appendix C: Sample MREOM Input File 87
Appendix D: MREOM Reference Weights and T Amplitudes per System 89

List of Figures

Figure 1: Definition of Slater Determinants 4
Figure 2: CAS Orbital Diagram 6
Figure 3: Example excitation of 1h1p out of the previously shown CAS 7
Figure 4: Excitations Included in a MRCISD calculation 8
Figure 5: Simplified Hamiltonian 10
Figure 6: Excitations remaining in our MREOM Calculation after transforming out the 2h, 2p, 1h2p, and 2p1h excitations. 11
Figure 7: MREOM-CC Calculation of $CoKr^+$ 13
Figure 8: CAS Energy Surface of Low Spin MnO^+ 23
Figure 9: Complete active space potential energy surfaces for high spin cases. 25
Figure 10: Complete active space potential energy surfaces for low spin cases. 26
Figure 11: Example T Amplitudes from a High Spin CoO^+ MREOM Calculation. 30
Figure 12: MREOM potential energy surface plots of MnO^+. 33
Figure 13: Comparison of SPT thresholds for Low Spin MnO^+ 35
Figure 14: Comparison of Energy values between differing SPT thresholds 36
Figure 15: MnO^+ calculated energy comparison at two selected points. 37
Figure 16: MREOM Potential Energy Surface Plots of FeO^+ 38
Figure 17: FeO^+ calculated energy comparison between spin cases. 39
Figure 18: MREOM potential energy surface plots of CoO^+. 40
Figure 19: MREOM Potential Energy Surface Plots of NiO^+ 41
Figure 20: Edited high spin NiO^+ potential energy surface 42
Figure 21: NiO^+ calculated energy comparison 43
Figure 22: MREOM potential energy surface plots of CrO^+. 44
Figure 23: CrO^+ calculated energy comparison. 45
Figure 24: Data Structure used in the new algorithm. 52
Figure 25: Structure of a matrix-matrix multiplication. 53
Figure 26: Example of array in memory 55

List of Tables

Table 1: Number of States below 2 eV for the Transition Metal Oxide systems in this study. 15
Table 2: Comparison of MREOM and NIST values for Transition Metal Atoms. 16
Table 3: Attempted High Spin CAS Configurations 18
Table 4: Attempted Low Spin CAS Configurations 18
Table 5: CAS Orbital Occupation Degeneracies of Low Spin MnO^+. 21
Table 6: CASSCF Energies of Low Spin MnO^+ Calculation at 1.65 Å. 22
Table 7: Failed MnO^+ CAS Calculation at 1.65 Å 23
Table 8: Successful CASSCF Calculation of MnO^+ at 1.65 Å 23
Table 9: MREOM calculation details including number of states, multiplicities, elapsed calculation time, and SPT threshold. 31
Table 10: Comparison of MREOM calculated bond lengths with literature 32
Table 11: Smallest references weights and largest T-amplitudes for high spin and low spin MnO^+. 34
Table 12: Smallest references weights and largest T amplitudes for low spin MnO^+ with SPT=0.05. 36
Table 13: MREOM results for VO^+. 46
Table 14: Relative timings of each calculation section for MREOM calculations in ORCA. 52
Table 15: Smallest References Weights and Largest T Amplitudes for MnO^+ 89
Table 16: Smallest References Weights and Largest T Amplitudes for FeO^+ 90
Table 17: Smallest References Weights and Largest T Amplitudes of CoO^+ 91
Table 18: Smallest References Weights and Largest T Amplitudes for NiO^+ 92
Table 19: Smallest References Weights and Largest T Amplitudes for CrO^+ 93

List of abbreviations

BLAS - Basic Linear Algebra Subroutines
CAS - Complete Active Space
CASSCI - Complete Active Space Configuration Interaction
CASSCF - Complete Active Space Self Consistent Field
CC - Coupled Cluster
CI - Configuration Interaction
DKH - Douglas– Kroll–Hess Hamiltonian
HF - Hartree Fock
MR - Multi Reference
MRCC - Multi Reference Coupled Cluster
MRCI - Multi Reference Configuration Interaction
MREOM - Multi Reference Equation of Motion
SPT – Singular Perturbation Theory
SR - Single Reference
1h - One Hole Excitation
1p - One Particle Excitation

Chapter 1

Introduction to Electronic Structure Theory

The electronic structure problem is one of the most basic problems within quantum chemistry. Many different theories and methods have been devised to solve this fundamental problem, with new methods arising to capture the structure of systems that fail using current approaches. The exact approach, the Full Configuration Interaction (FCI) method, can involve solving equations with billions of determinants for a molecule as simple as ethylene [1]. Solving eigenvalue equations with this incredibly large dimension is not feasible with current technology. For this reason, we look to methods that reasonably approximate properties of interest which can be implemented using modern hardware.

Single reference (SR) calculations are often the starting point for electronic structure theory calculations, and usually work well for systems starting relatively close to their equilibrium geometry, if they have a wavefunction that can be described by a single slater determinant. The Hartree-Fock method [2] is a common single reference calculation included in most, if not all, quantum chemistry software packages. The Hartree-Fock method is an excellent method when determining ground state geometries as well as vibrational frequencies. This method can yield 99.9% of the total electronic energy of the system in Hartrees. However, for a small molecule such as H_2O even a difference as small as 0.1% yields error in the total energy of around 300 kJ/mol, or 50 kcal/mol. A large fraction of the error can be expected to cancel when evaluating reaction energies, but in general Hartree-Fock does not calculate accurate enough energies. A method that goes beyond the simplified treatment of the Hartree-Fock approximation is required to treat more complicated systems. Coupled Cluster (CC) [3] theory is a common method beyond Hartree-Fock. This method yields much better accuracy for electronic energies (1 kcal/mol) but is a single reference method, and once again is only applicable if the wavefunction of the system can be qualitatively described by a single determinant. In the cases of low lying excited states, transition metal compounds,

cases including bond-breaking, and magnetic or spin state systems, the single reference approximation is often not accurate. In these instances, we must use multiple determinants to describe our wave-function, even qualitatively.

Multireference (MR) methods become necessary when single reference methods fail to approximate the electronic structure of a system in question. Implementations of this multi-reference approximation include Multireference Configuration Interaction (MRCI) [4], Multireference Coupled Cluster (MRCC) [5], as well as the Multireference Equation of Motion (MREOM) [6] method, developed in the Nooijen group to reduce the cost of multi-reference calculations while calculating hundreds of states simultaneously. In this proposal, the primary multi reference method employed will be MREOM. MREOM has been successful as a method for determining the electronic structure of problematic atoms and small molecules. This method involves a Complete Active Space (CAS) specification, where many open shell orbitals and electrons to be distributed to these orbitals are specified. The active space is much smaller than the complete orbital space. Therefore, full CI calculations within the CAS space are feasible. This is called CASCI. In addition, when the orbitals that define the CAS are optimized the calculations are referred to as CASSCF. This compact CAS gives rise to many reference determinants, in which different electronic state configurations are accounted for. After specifying the reference space, a series of careful transformations can be applied to the bare Hamiltonian, which simplifies the resulting diagonalization while preserving the Hamiltonians original eigenvalues, or energy values. MREOM has been used to calculate atomic excitation spectra for transition metals such as Cr, Mn, Fe, and Co [7], transition metal complexes [8], and large numbers of valence excited states for organic compounds [9]. While MREOM has seen great success as a more time-economical alternative to other multi-reference methods, MREOM is still under development. Advances can be made on the algorithm's implementation to significantly speed up computation time.

In this thesis, the current theory behind MREOM will be explained, detailing how transformations can be made to the Hamiltonian such that the calculation becomes more efficient while also becoming more accurate [9]. Applications of MREOM to six diatomic transition metal oxide cations are proposed as interesting test systems well suited to challenge MREOM. These systems are electronically complicated due to the presence of many low-lying states. Calculating potential energy surfaces for these systems is challenging, and a calculation approach is proposed to simplify the process. Finally, a new implementation for MREOM is proposed. This new method combines an intelligent data structure with optimized linear algebra subroutines to calculate many energy states simultaneously, leading to large theoretical speed ups in calculation time. These changes have not been implemented fully due to time constraints. Sample code used for each Hamiltonian contribution for both the one body and two body case are examined in detail, and the next steps required to finish the project are outlined.

Chapter 2

Multi-Reference Equation of Motion Coupled Cluster Theory

The electronic structure problem is the solution to the wave-function of electrons in an electrostatic field created by stationary nuclei. These nuclei are considered fixed due to the assumption that motion of nuclei and electrons can be separated due to the different time scales these motions occur on, using the Born-Oppenheimer approximation. This solution involves both the wave function of the electrons as well as their energies. Slater determinants [10] are used as an expression for these multi-electron systems, since they satisfy the anti-symmetry requirements of the wave-function, which in turn satisfies the Pauli exclusion principle. These properties are outlined in *Figure 1*.

$$\psi_\lambda = \frac{1}{\sqrt{N!}}\begin{vmatrix} \chi_1(x_1) & \chi_2(x_1) & \cdots & \chi_N(x_1) \\ \chi_1(x_2) & \chi_2(x_2) & \cdots & \chi_N(x_2) \\ \vdots & \vdots & \ddots & \vdots \\ \chi_1(x_N) & \chi_2(x_N) & \cdots & \chi_N(x_N) \end{vmatrix} \equiv |\chi_1\chi_2 \cdots \chi_N|$$

$$|\chi_1\chi_2 \cdots \chi_N| = (-1)|\chi_2\chi_1 \cdots \chi_N|$$

$$|\chi_1\chi_1 \cdots \chi_N| = 0$$

Figure 1: Definition of Slater Determinants, including built in anti-symmetry and Pauli exclusion properties

Currently most wave-function based Quantum Chemistry problems are phrased in the language of Second Quantization [10]. The benefit of Second Quantization is that the slater determinants can be represented by a series of operators, and the problem will be reduced to algebra manipulations. The problem can then be easily programmed and solved via computation. We specify the wave-function as a series of ordered orbitals with occupation numbers zero or one denoting whether the orbital contains an electron or not. Equation 1 shows a sample wave-function with N electrons. The notation indicates that orbitals a, d, and z are occupied.

$$|a_1, b_0, c_0, d_1, \dots, z_1\rangle \tag{1}$$

Two major operators exist in second quantization. The first is the creation operator $\hat{p}^\dagger$, which adds an electron to orbital p. The second is the annihilation operator which removes an electron from orbital p. The Hamiltonian written using Second Quantization is shown below. It has been written with only one and two particle excitations.

$$\widehat{H} = h_q^p \hat{p}^\dagger q + h_{pq}^{rs} \hat{p}^\dagger \hat{q}^\dagger rs \tag{2}$$

$$h_q^p = \int \varphi_p^*(\tau) \left[-\frac{1}{2}\nabla^2 + V^{H_l}\left(\overrightarrow{r_\phi}\right) \right] \varphi_q(\tau) d\tau \qquad \tau = (\vec{r}, \phi) \tag{3}$$

$$h_{pq}^{rs} = \langle pq|rs\rangle - \langle pq|sr\rangle \tag{4}$$

$$\langle pq|rs\rangle = \int\int \varphi_p^*(\tau_1)\varphi_q^*(\tau_2) \frac{1}{|\overrightarrow{r_1} - \overrightarrow{r_2}|} \varphi_r(\tau_1)\varphi_s(\tau_2) d\tau 1 d\tau 2$$

From here, we can discuss the Full Configuration Interaction (CI) problem. This involves including every Slater determinant expressing excitations from our ground state electronic configuration into any number of virtual orbitals. If we have N_a and N_b alpha and beta spin orbitals as well as M spatial orbitals, we have $\binom{M}{N_a}\binom{M}{N_b}$ determinants, each of which is an eigenstate of a one electron Hamiltonian. This can be used as the basis for our many electron problem. We then write:

$$|\Psi\rangle = \sum_\lambda C_\lambda |\phi_\lambda\rangle \tag{5}$$

We then apply the variational principle to the above:

$$E = \frac{\langle \Psi|H|\Psi\rangle}{\langle \Psi|\Psi\rangle} \tag{6}$$

Which then leads to the eigenvalue problem:

$$\sum_{\mu}\langle\Psi_{\lambda}|H|\Psi_{\mu}\rangle\, C_{\mu} = EC_{\lambda}$$
$$HC = CE \tag{7}$$

CI may also be undertaken as a multi reference calculation, referred to as MRCI. The driving principle behind Multi Reference calculations involves defining a Complete Active Space (CAS) in terms of occupied orbitals, active orbitals, and virtual orbitals. This is done using a CAS Self Consistent Field (CASSCF) calculation. The goal is to optimize the orbitals such that $\mathrm{E_{CAS}}$ is minimized. The CAS is defined as a linear combination of determinants with a set of coefficients to be optimized as shown in equation 8.

$$|CAS\rangle = \sum_{\lambda} C_{\lambda}|\phi_{\lambda}^{CAS}\rangle \tag{8}$$

As stated previously, our CAS is comprised of three different types of orbitals [11]; occupied orbitals which are each doubly occupied, virtual orbitals which are empty, and active orbitals that can be populated with zero, one, or two electrons. *Figure 2* shows an example CAS. Each determinant in the CAS-space will have an identical core occupied space but differ in the configuration of electrons in the active orbitals. An example CAS is given in *Figure 2*, while an example excitation removing an electron from this CAS can be seen in *Figure 3*.

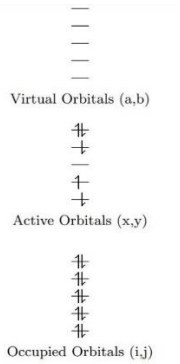

Figure 2: CAS Orbital Diagram Showcasing doubly occupied orbitals (Occupied), variably occupied orbitals (Active), and empty orbitals (Virtual).

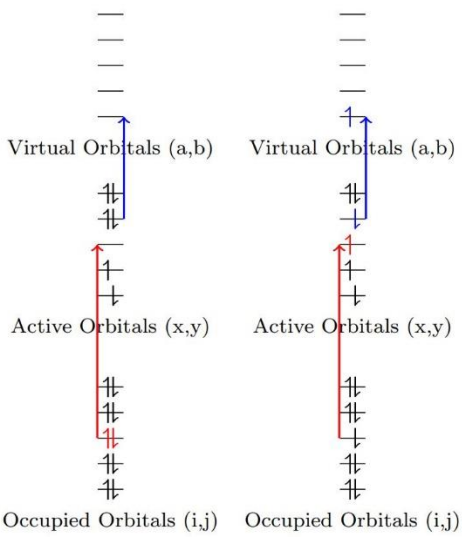

Figure 3: Example excitation of 1h1p out of the previously shown CAS. An electron from an occupied orbital is promoted to an active orbital, while simultaneously an electron from an active orbital is promoted to a virtual orbital.

The different excitations occurring outside of the CAS will be referred to as follows. Excitations that involve an electron being promoted from an occupied orbital will be referred to as a hole (h) excitation. Excitations that involve an electron being promoted to a virtual orbital will be referred to as a particle (p) excitation. The following are the list of excitations included in Multi Reference Configuration Interaction with Singles and Double excitations (MRCISD). These excitations are visualized in *Figure 4.*

1. 1 hole(1h): An electron from an occupied orbital is promoted to the active space
2. 1 particle(1p): An electron is promoted from the active space to a virtual orbital
3. 1h1p: An electron from an occupied orbital is promoted to a virtual orbital; electron is promoted from an occupied orbital to an active orbital, and an electron from an active orbital is promoted to a virtual orbital.
4. 2p: Two electrons from the active space are promoted to the virtual orbitals.
5. 2h: Two electrons from the occupied orbitals are promoted to the active space.
6. 2h 1p: Two holes are created in the occupied space, and a particle is added to the virtual space

7. 1h 2p: One hole is created in the occupied space, and two particles are created in the virtual space.

8. 2h 2p: Two holes are created in the occupied space, and two particles are created in the virtual space.

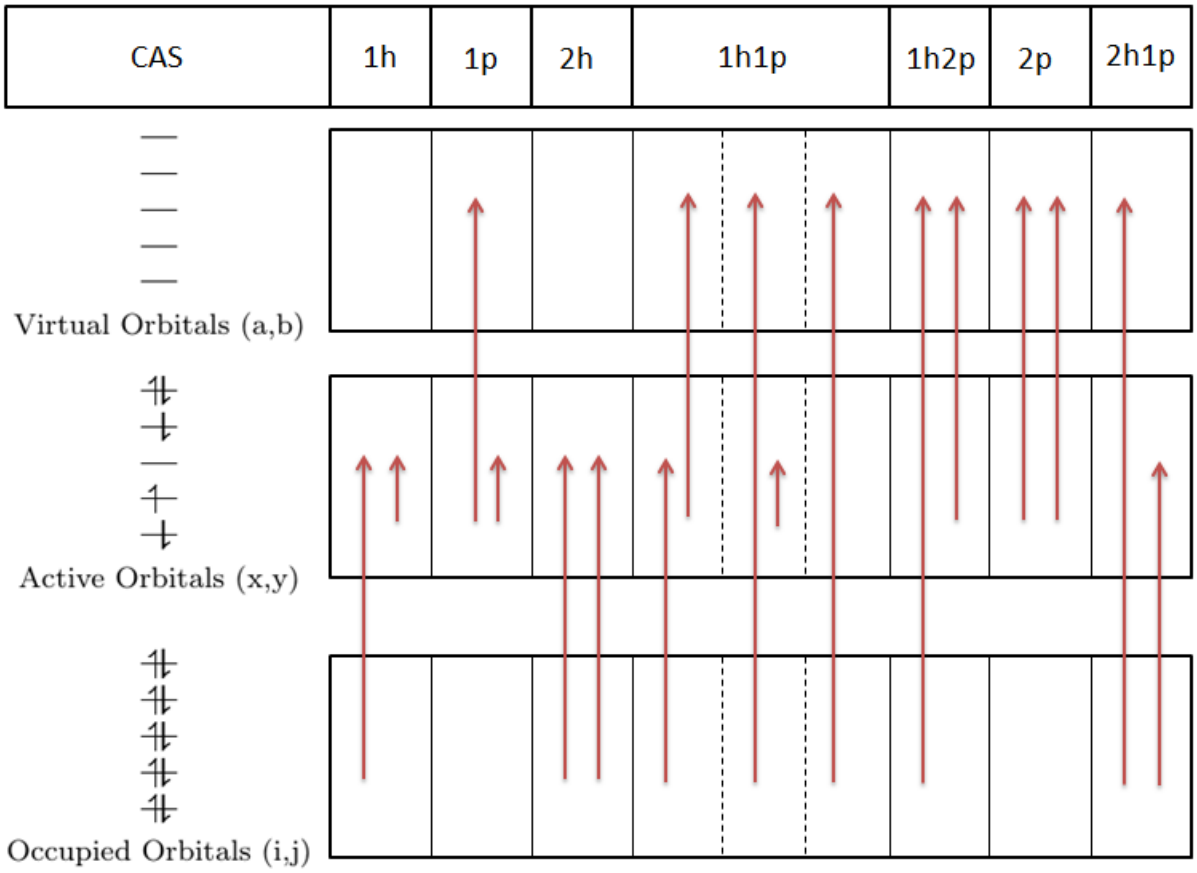

Figure 4: Excitations Included in a MRCISD calculation. These excitations may potentially include active-active excitations in addition to the labeled excitation which do not change the overall excitation.

While the above seems reasonable, in practice it is only usable for small molecules. Once again, the number of determinants scales as $n_h^2\ n_p^2 \mathrm{n_{CAS}}\ [12]$. $\mathrm{n_{cas}}$ may be as large as ~100,000, therefore MRCI calculations have the capacity to be incredibly expensive. Using modern technology, it is impossible to store and compute this incredible number of determinants. For this reason, full MRCISD is only used for

small active spaces. A more widely used alternative is internally contracted MRCI. The main drawback to this method is a lack of size extensivity, which in practice means that large active spaces must be used.

The Multi Reference Equation of Motion method for electronic structure calculations can be described, in broad terms, as a series of transformations to a bare Hamiltonian ($\hat{H}$) that is then followed by a diagonalization to the final transformed Hamiltonian ($\hat{G}$). Once our CAS has been determined as previously outlined, we can then build and transform our Hamiltonian. Starting from the Schrödinger equation, we can apply a transformation to our Hamiltonian as in equation 9.

$$\hat{G} = U^{-1}\hat{H}U \tag{9}$$

We then show in equation 10 that transforming our Hamiltonian in principle only changes our eigenvectors and not our eigenvalues. This means that any transformation we apply to our Hamiltonian will not change the results of our MREOM calculation. The goal of this transformation is to decouple the CAS from the external space as indicated in Equation 11.

$$\hat{G}|\Phi_\lambda\rangle = \left(U^{-1}\hat{H}U\right)(U^{-1}|\Psi_\lambda\rangle) \tag{10}$$

$$\hat{G}|\Phi_\lambda\rangle = U^{-1}\hat{H}|\Psi_\lambda\rangle$$

$$\hat{G}|\Phi_\lambda\rangle = U^{-1}|\Psi_\lambda\rangle E_\lambda$$

$$\hat{G}|\Phi_\lambda\rangle = |\Phi_\lambda\rangle E_\lambda$$

$$\langle\phi_X|\hat{G}|\phi_{CAS}\rangle = 0 \tag{11}$$

If we could apply transformations to the Hamiltonian such that equation 11 holds, the final diagonalization would be very compact, and only include CAS configurations as illustrated in Equation 12. Once we have the transformed Hamiltonian, we multiply this resulting matrix by a column vector C that

satisfies equation 12 and preserves our eigenvalues. At this point, only excitations within our CAS remain as shown in *Figure 5.*

$$\begin{array}{c} \\ CAS \\ X \end{array} \begin{array}{c} \begin{array}{cc} CAS & X \end{array} \\ \begin{bmatrix} A & B \\ 0 & D \end{bmatrix} \end{array} \begin{bmatrix} C \\ 0 \end{bmatrix} = \begin{bmatrix} A \times \mathrm{C} \\ 0 \end{bmatrix}$$

Figure 5: Simplified Hamiltonian obtained after removing all excitations out of the CAS.

$$AC_\lambda = C_\lambda E_\lambda \tag{12}$$

While the above is conceptually possible, we find that excluding all the excitations out of the CAS results in poor results. For this reason, we still include 1h, 1p, and sometimes 1h1p excitations in our calculation. Using Second Quantization, we perform a series of transformations to remove unwanted excitations out of the CAS. Our transformations all have a similar form, and the example given below is of the ”T” transformation.

$$\bar{H} = e^{-T} H e^{T} \tag{13}$$

$$\bar{H} = \bar{h}_0 + \bar{h}_p^q \{\hat{e}_q^p\} + \bar{h}_{pq}^{rs} \{\hat{e}_{rs}^{pq}\} + \bar{h}_{pqr}^{stu} \{\hat{e}_{stu}^{pqr}\} + \cdots$$

$$\hat{e}_q^p = \hat{p}^\dagger \hat{q}$$

$$\hat{e}_{rs}^{pq} = \hat{p}^\dagger \hat{q}^\dagger \hat{s} \hat{r}$$

T amplitudes are then solved via Equation 14, where ω_k and R_k denote the weights used and states from the CASSCF calculation, and i/x denotes an active or inactive orbital. The notation {...} is technically involved, and it denotes Kutzelnigg-Mukherjee normal ordering [13] for a multi-configurational reference. Moreover, the many-body transformations introduce three body interactions in $\hat{G}$, which are assumed

small. However, this implies that results are always approximate since the three body elements are neglected as shown in Equation 13. We denote three other similarity transforms $\hat{S}$, $\hat{X}$ and $\hat{D}$ in a similar fashion in Equation 15.

$$\sum_k \omega_k \left\langle R_k \middle| E_a^{\frac{i}{x}} \bar{H} \middle| R_k \right\rangle = 0 \tag{14}$$

$$\bar{h}_{ij}^{ab} = \bar{h}_{ix}^{ab} = \bar{h}_{xy}^{ab} = 0$$

$$\bar{G} = \{e^{S+X=D}\}^{-1} \bar{H} \{e^{S+X=D}\} \tag{15}$$

$\hat{G}$ is our Hamiltonian with all excitations involving more than two bodies removed. This approximation is applicable assuming that contributions due to three body or more terms are negligible. *Figure 6* shows an example structure of the two body equations in $\hat{G}$ over the CAS + 1h + 1p determinants.

	CAS	1h	1p	1h1p
CAS	e_{tu}^{xy}	e_{xu}^{iy}	e_{au}^{xy}	e_{ay}^{xi}
1h	e_{iu}^{xy}	e_{ju}^{ix}	e_{ia}^{xu}	e_{ia}^{ju}
1p	e_{tu}^{ay}	e_{xy}^{ia}	e_{by}^{ax}	e_{ax}^{bi}
1h1p	e_{xi}^{ay}	e_{ju}^{ia}	e_{bi}^{ax}	e_{bj}^{ai}

Figure 6: Excitations remaining in our MREOM Calculation after transforming out the 2h, 2p, 1h2p, and 2p1h excitations.

We then diagonalize this final more compact space as outlined in MRCI. Of note are the huge gains in efficiency in MREOM versus MRCI by reducing the number of determinants in the final diagonalization by several orders of magnitude. However, the most expensive step in current MREOM calculations is still this final diagonalization. Future steps are to be taken to increase the efficiency of diagonalization to speed up the slowest part of the current MREOM implementation.

Chapter 3

Multi-Reference Equation-Of-Motion Study of MO^+

(M = V, Cr, Mn, Fe, Co, Ni)

In the previous chapter, an overview of electronic structure theory was discussed leading to the theory behind a particular multi-reference method: Multi-Reference Equation of Motion Coupled Cluster (MREOM-CC). MREOM-CC has been previously used in studies to calculate transition metal atom spectra [7], vertical excitation spectra from organic molecules as well as transition metal complexes [14], model magnetic systems, as well as potential energy surfaces where single reference methods failed. *Figure 7* shows the result of an MREOM calculation of $CoKr^+$. In this study some 200 excited states were calculated by MREOM. [15]

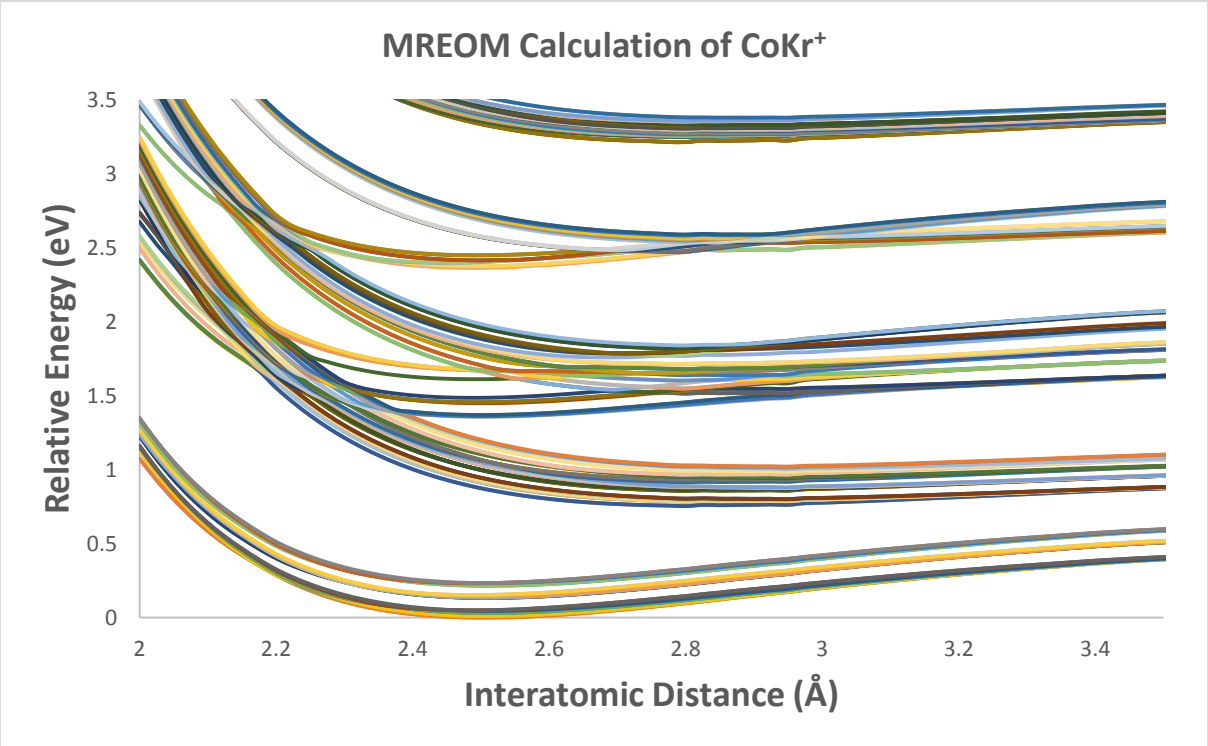

Figure 7: MREOM-CC Calculation of $CoKr^+$ including approximately 200 States with corrections for Basis Set Superposition Error (BSSE). This calculation was not possible with single reference methods and gives an idea of the capabilities of MREOM.

The main strength of MREOM is the ability to calculate many excited states from a single set of amplitudes as well as a state averaged CAS. These amplitudes and the nature of this state averaged CAS were discussed in the previous chapter. In this chapter, the principles behind running a CASSCF and MREOM calculation in the ORCA program are described. A study will be conducted to calculate the potential energy surfaces of six cations of transition metal oxides using MREOM. Currently the most successful method to calculate potential energy surfaces is MRCI(+Q) [16]. The method is robust due to a variational wavefunction and a state specific approach. In this chapter the suitability of using MREOM as a method to calculate potential energy surfaces will be explored.

3.1: Systems in Study: Transition Metal Oxide Cations

The systems under consideration are several positively charged diatomic transition metal oxides (MO^+, M = V, Cr, Mn, Fe, Co, Ni). These systems were chosen for two key reasons. The MREOM approach has been used to calculate potential energy surfaces for only a few systems, notably $CoKr^+$ and $CoAr^+$ These systems are comparatively simple. The transition metal oxides are far more challenging to calculate, and this study provides a more stringent challenge for the methodology. The second reason these systems were chosen was that the proposed systems of this computational study lend themselves easily to experimentation via Velocity Map Imaging (VMI) in the Hopkins lab [17]. To attempt to gauge the number of states in each system, excited state energy levels were taken from NIST for each transition metal atom and for the lowest three energy levels of oxygen. While each transition metal atom is densely packed with many low lying excited states, oxygen has a gap of almost ~2 eV. However, that metal coupled to oxygen will have nine times that due to the coupling of states between the transition metal and oxygen's ^3P states. At the asymptote of the potential energy surface, the energy of the system can be represented as:

$$E(MO^+) = E(M^+) + E(O)$$

Table 1 shows the number of states that can be expected under 2 eV for each system based on the coupling of energy state values taken from NIST [18]. While each system has many low-lying states, VO^+ deserves special mention due to the relatively high density of states at low energy. Potential energy surfaces were found for each system, except VO^+. This may be due in part to the added complexity of the system compared to the other systems studied; VO^+ has by far the highest density of low lying states in the asymptote regime.

Table 1: Number of States below 2 eV for the Transition Metal Oxide systems in this study.

VO^+	CrO^+	MnO^+	FeO^+	CoO^+	NiO^+
252	54	63	153	135	72

As a quick comparison, values from NIST can be compared to bare atom MREOM calculations including spin orbit coupling for the first three term symbols, shown in *Table 2*. These MREOM energy values have been lined up to the term symbols and J values of each energy level. The average of states at an energy level is compared to the given NIST values. In most cases this absolute error is small, with high absolute error offset by a low percent difference. Even when only including the first three term symbols, each transition metal cation has many densely packed states. This simple comparison makes the electronic complexity of the transition metals apparent.

While the energies of the states at asymptotes can be calculated using the above and compared with MREOM calculations, there isn't a simple way to calculate energies near equilibrium geometries. However, the character of these states changes as the bonds of the system are broken. Equilibrium structures can be pictured as a combination of M^{3+} and O^{2-}.

Table 2: Comparison of MREOM and NIST values for Transition Metal Atoms.

Atom	Electron Configuration	Term	J	NIST (eV)	Average Level Energy (eV)	Absolute Difference (eV)	Percent Difference
V^+	$3d^4$	^5D	0	0	0	0	N/A
			1	0.0045	0.0052	0.0008	17.23%
			2	0.0132	0.0156	0.0023	17.66%
			3	0.0259	0.0306	0.0047	18.34%
			4	0.0421	0.0501	0.0081	19.18%
	$3d^3\,4s$	^5F	1	0.323	0.2653	0.0577	17.86%
			2	0.3331	0.2765	0.0566	16.99%
			3	0.3482	0.2934	0.0548	15.75%
			4	0.368	0.3157	0.0523	14.22%
			5	0.3921	0.3433	0.0488	12.46%
	$3d^3\,4s$	^3F	2	1.0713	0.89	0.1812	16.92%
			3	1.0963	0.918	0.1783	16.26%
			4	1.128	0.954	0.1739	15.42%
Cr^+	$3d^5$	^6S	5/2	0	0	0	N/A
	$3d^4\,4s$	^6D	1/2	1.4831	1.4521	0.031	2.09%
			3/2	1.4918	1.4618	0.0301	2.02%
			5/2	1.5061	1.4778	0.0284	1.88%
			7/2	1.5255	1.4997	0.0258	1.69%
			9/2	1.5494	1.5273	0.0221	1.42%
	$3d^4\,4s$	^4D	1/2	2.4212	2.2103	0.2108	8.71%
			3/2	2.434	2.2251	0.2088	8.58%
			5/2	2.4546	2.249	0.2056	8.38%
			7/2	2.4827	2.2808	0.2018	8.13%
Mn^+	$3d^5\,4s$	^7S	3	0	0	0	N/A
	$3d^5\,4s$	^5S	2	1.1745	1.0773	0.0972	8.28%
	$3d^6$	^5D	4	1.7762	2.1694	0.3932	22.14%
			3	1.8094	2.1996	0.3902	21.56%
			2	1.8326	2.2223	0.3896	21.26%
			1	1.8475	2.2374	0.3899	21.10%
			0	1.8548	2.245	0.3902	21.04%
Fe^+	$3d^6\,4s$	^6D	9/2	0	0.002	0.002	N/A
			7/2	0.0477	0.0466	0.0011	2.27%
			5/2	0.0828	0.0798	0.003	3.64%
			3/2	0.107	0.1028	0.0042	3.92%
			1/2	0.1211	0.1163	0.0048	3.96%
	$3d^7$	^4F	9/2	0.2322	0.5056	0.2734	117.77%
			7/2	0.3013	0.5713	0.27	89.60%
			5/2	0.3519	0.6213	0.2694	76.56%
			3/2	0.3865	0.6581	0.2716	70.26%
	$3d^6 4s$	^4D	7/2	0.9863	0.9439	0.0424	4.30%
			5/2	1.0405	0.9958	0.0447	4.29%
			3/2	1.0762	1.0299	0.0463	4.30%
			1/2	1.0969	1.0494	0.0475	4.33%
Co^+	$3d^8$	^3F	4	0	0.0002	0.0002	N/A
			3	0.1178	0.1142	0.0037	3.11%
			2	0.198	0.1924	0.0057	2.86%
	$3d^7\,4s$	^5F	5	0.4154	0.3109	0.1045	25.15%
			4	0.4995	0.3912	0.1083	21.69%
			3	0.5655	0.4558	0.1097	19.39%
			2	0.6137	0.5042	0.1095	17.85%
			1	0.6453	0.5364	0.1089	16.88%
	$3d^7\,4s$	^3F	4	1.2166	1.0853	0.1313	10.79%
			3	1.3277	1.1934	0.1343	10.12%
			2	1.4037	1.2668	0.1369	9.76%
Ni^+	$3d^9$	^2D	5/2	0	0.0006	0.0006	N/A
			3/2	0.1868	0.185	0.0018	0.96%
	$3d^8\,4s$	^4F	9/2	1.0407	1.1339	0.0932	8.96%
			7/2	1.1568	1.2472	0.0904	7.82%
			5/2	1.2542	1.3428	0.0886	7.07%
			3/2	1.3222	1.4099	0.0878	6.64%
	$3d^8\,4s$	^2F	7/2	1.68	1.7579	0.0778	4.63%
			5/2	1.8592	1.9343	0.075	4.04%

When looking at the above, it is important to decide when to consider absolute difference as opposed to percent difference. In certain cases, states have large percent differences with an absolute difference of less than ~0.1 eV. In some cases, both percent difference and absolute difference are high. Due to the restriction of using a single CAS for all states, MREOM calculations are not always accurate for all atomic states. Errors occur in the above energy level calculations due to the supplied CAS not containing states with the correct character. While the solution would be to add in another set of states with the proper character, it is complicated to find a correct state averaged CAS over many states. This issue may be more complicated for molecules. Near equilibrium the bonding solution of MO^+ can be described formally as $M^{3+} + O^{2-}$. As the geometry changes to larger interatomic distances, this will shift to the asymptote of $M^+ + O$. The electronic structure must capture this change in character.

3.2: Calculation Strategy: 'High spin' and 'Low spin'

The essence of the approach used for this study was to attempt to distill the CAS of each calculation into two separate categories: (i) using the highest possible allowed spin case by maximizing the number of unpaired electrons and (ii) a more moderate spin case where different configurations of the CAS were explored. The high spin case was chosen to simplify the CAS process, whereas the low spin cases were chosen as an alternative in the event at the high spin cases failed. These regimes were chosen to simplify the CAS selection process, removing the option of mixed spin active spaces. In the end, calculations from both approaches ended up both succeeding and failing, with certain transition metal cations proving to be more complicated than others.

Six species were chosen to be studied; VO^+, CrO^+, MnO^+, FeO^+, CoO^+, and NiO^+. These transition metals are all in the same row of the periodic table, and are adjacent in atomic number. This was done to examine the differences in electronic structure between similar species, as well as the effects this had on various calculation properties such as overall calculation timings. *Table 3* and *Table 4* denote the CAS's used for

each molecule. In the following tables, red denotes that the calculation failed, and green denotes that it has succeeded. In all cases, a CAS could be found that appeared continuous, but the MREOM calculation might still fail. Reasoning for this will be touched on later.

Table 3: Attempted High Spin CAS Configurations, *with successful configurations in green and failed configurations in red.*

		High Spin		
System	**Electrons**	**Orbitals**	**Multiplicity**	**States**
VO^+	8	9	9	5
	8	8	9	5
CrO^+	9	9	10	1
MnO^+	10	9	9	5
FeO^+	11	9	8	5
CoO^+	12	9	7	5
NiO^+	13	9	6	4

Table 4: Attempted Low Spin CAS Configurations, with successful configurations in green and failed configurations in red.

		Low Spin		
System	**Electrons**	**Orbitals**	**Multiplicity**	**States**
VO^+	8	8	3	1
	8	8	3	3
	7	6	5	3
	8	8	3,1	5,5
CrO^+	9	8	4	3
	9	8	4	2
MnO^+	10	9	5	3
FeO^+	11	9	6	3
CoO^+	12	9	5	2
NiO^+	13	9	4	3

3.3: Basics of Complete Active Space Calculations

A proper CASSCF calculation is the first step to an MREOM calculation. For an MREOM calculation to be successful, there are certain requirements for the calculated CAS. One would wish to define a single state-averaged CAS that results in continuous, symmetry adapted results over the whole range of requested geometries. Unfortunately, the CASSCF implementation in ORCA does not allow for explicit definitions of symmetry within the CAS. The only control the user has over CAS symmetry is to check degeneracy patterns upon convergence which occurs at two levels.

The first level is to check the converged orbital degeneracies, both of orbital energies and of orbital occupation numbers. There are two possible degeneracy patterns for orbitals in the proposed systems. π, δ, and ϕ orbitals are doubly degenerate, while σ orbitals are non-degenerate. The second quality check is to check the degeneracy of calculated states. The same capitalized labels Π, Δ, Φ, and Σ characterize electronic states. Π, Δ, Φ all refer to doubly degenerate states whereas Σ refers to non-degenerate states. At the CASSCF computation level it is important to ensure that complete multiplets are included in the CAS. When running CASSCF calculations using ORCA, all of this must be judged using degeneracy patterns. Including incomplete multiplets will result in incorrect degeneracy patterns.

A CASSCF calculation is defined by the number of electrons in the system, the orbitals that these electrons will populate over different state averaged configurations, the multiplicities to be calculated, and the number of states to be calculated for each multiplicity [19]. This step is the most user intensive step; there is currently no automated way to set up the active space. While the number of orbitals and electrons is given by the system at the start of the equation, this can change as ‘problem’ orbitals arise. This will be discussed in greater detail later.

The following is a sample CASSCF ORCA input:

```
!CASSCF DKH ma-DKH-def2-TZVP

* xyz 1 4
Ni 0.000000 0.000000 0.000000
O 0.000000 0.000000 1.650000
end


%casscf
nel 10
norb 9
mult 5
nroots 3
end
```

The calculation's appearance is deceptively simple. The first line denotes the type of calculation and basis set to be used, with available basis sets being found in the ORCA manual [20]. 'DEF2-TZVP' is a minimally augmented basis set designed for heavy metal elements, while the 'ma' tag denotes that a subsection of elements contain a minimal set of diffuse functions [21]. DKH denotes the use of a Douglas–Kroll–Hess Hamiltonian for scalar relativistic effects [22]. The next block denotes the geometry of the system, including the XYZ coordinates of every atom in the calculation. Finally, the CASSCF block lists all required pieces of the calculation. Note that there are several default settings not listed in the above that may be changed as the need arises. These can be found in the ORCA manual.

Table 5 contains the first user check of a completed CASSCF calculation, the orbital degeneracy patterns. When summed across, each row in this table will equal the number of electrons specified for the active space. This table lists the expected value of electrons that exist in each given orbital. The expectation is that a clear degenerate pattern will exist in the set of active orbitals. *Table 5* shows the orbital degeneracy of MnO^{+} over an interatomic distance of 1.45 to 2.00. Each row of the table represents a different geometry.

Table 5: CAS Orbital Occupation Degeneracies of Low Spin MnO^+.

Interatomic Distance (Å)	State Averaged Orbital Occupancy								
1.4	1.9089	1.9089	1.9009	1.0003	1.0003	0.7575	0.7575	0.7105	0.0553
1.45	1.8888	1.8888	1.8886	1.0004	1.0004	0.7775	0.7775	0.7251	0.053
1.5	1.8747	1.8651	1.8651	1.0003	1.0003	0.8011	0.8011	0.7426	0.0496
1.55	1.859	1.8385	1.8385	1.0003	1.0003	0.8277	0.8277	0.7627	0.0455
1.6	1.8413	1.8105	1.8105	1.0002	1.0002	0.8556	0.8556	0.7849	0.0412
1.65	1.8219	1.7831	1.7831	1.0001	1.0001	0.8829	0.8829	0.8088	0.0372
1.7	1.8015	1.7585	1.7585	1	1	0.9074	0.9074	0.833	0.0338
1.75	1.7809	1.7379	1.7379	0.9999	0.9999	0.9279	0.9279	0.8561	0.0315
1.8	1.7609	1.7216	1.7215	0.9999	0.9999	0.9442	0.9442	0.8771	0.0307
1.85	1.742	1.709	1.709	0.9999	0.9999	0.9567	0.9567	0.8954	0.0316
1.9	1.7243	1.6994	1.6994	0.9998	0.9998	0.9662	0.9662	0.9109	0.0339
1.95	1.7074	1.6919	1.6919	0.9998	0.9998	0.9735	0.9735	0.9238	0.0383
2	1.6909	1.686	1.686	0.9998	0.9998	0.9793	0.9793	0.9342	0.0447

In the above table there is a clear orbital degeneracy pattern in each calculation. The above calculation looks good, but an MREOM calculation run with the above CAS would most likely result in T amplitudes that are not converged. This is due to the last orbital in the CAS having a very low orbital occupancy (<0.05) throughout most of the CAS energy surface. This issue can be solved by altering the CAS to the CAS found below. By removing the problem orbital, the occupancy is distributed among the remaining 8 orbitals. However, problems with T amplitude convergence also occur if an orbital is too highly populated (>1.95). This can be solved by removing two electrons in addition to removal of the orbital.

```
%casscf
nel 10
norb 8
mult 5
nroots 3
```

The second check performed is to ensure the degeneracy of the calculated states. Once again, it is expected for these states to either be non-degenerate or doubly degenerate. *Table 6* shows a degeneracy pattern denoting appropriate orbital symmetry within the CAS calculation.

Table 6: CASSCF Energies of Low Spin MnO^+ Calculation at 1.65 Å.

Energy (Ha)	Relative Energy (eV)
-1231.9966	0
-1231.9966	0
-1231.9692	0.7467

The issue with orbital occupancies that approach either doubly occupied or empty orbitals is that operators related to these orbitals carry a low weight; this makes it difficult to describe the amplitudes related to those operators. When calculating CAS excitations, highly occupied orbitals will be difficult to excite into, whereas lowly occupied orbitals are difficult to excite out of. In general, finding appropriate orbital degeneracies will lead to proper energy degeneracies, but this is not a guarantee. It's important to always check both the degeneracies of the orbitals and the degeneracies of the calculated states. When running calculations on diatomic metal cations, it can be common to 'split' a degeneracy by only including one of the two states from the degeneracy. This will result in a set of orbitals without symmetry. The following calculation results found in *Table 7* include one state from a multiplet. *Table 8* shows the calculation result that occurs after including the missing half of the multiplet. This calculation can be further improved by the removal of the low occupancy orbital. Of note in the above is that adding and removing states shifts the calculated energies of the same states between calculations.

Table 7: Failed MnO^+ CAS Calculation at 1.65 Å with number of states set to 1. This calculation failed due to the inclusion of a split multiplet.

State Energy (Ha):	-1232.0028
Orbital Occupancy	
1.9809	
1.9436	
1.5409	
1.0176	
1.0084	
1.0002	
1.0001	
0.4605	
0.0479	

Table 8: Successful CASSCF Calculation of MnO^+ at 1.65 Å after including the other half of the chosen multiplet by setting number of states to 2.

State Energies (Ha):	-1231.9998 -1231.9998
Orbital Occupancy	
1.9447	
1.7003	
1.7003	
1.0081	
1.0003	
1.0003	
0.7997	
0.7997	
0.0468	

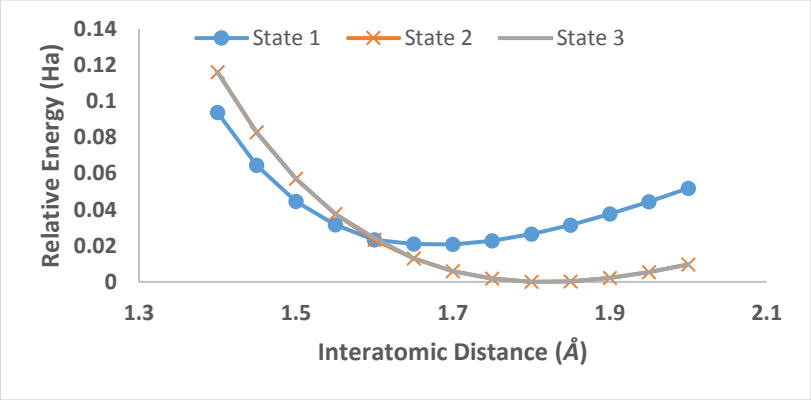

Figure 8: CAS Energy Surface of Low Spin MnO^+. The surfaces appear smooth, with two calculated states appearing degenerate.

Figure 8 shows the result of a CAS energy surface of MnO^+, calculating 3 energy states with a multiplicity of 5. States 2 and 3 are degenerate, and are denoted with square points as opposed to circular. The continuous and well-behaved nature of the calculated surface means that this CAS is a prime candidate for an MREOM calculation. While the above is a good set of rules to start from when attempting a CASSCF calculation, finding the proper CAS is the first step to an MREOM calculation. Unfortunately, a good CAS does not guarantee the success of a MREOM calculation.

3.4: CASSCF Calculation Results and Discussion

Figure 9 and *Figure 10* show the potential energy surfaces calculated for each CAS used for an MREOM calculation as well as the orbital occupancies related to that CAS. Each calculation was conducted using the ma-DKH-Def2-TZVP basis set. Tables covering orbital occupancies can be found in Appendix B.

High Spin CAS Potential Energy Surfaces

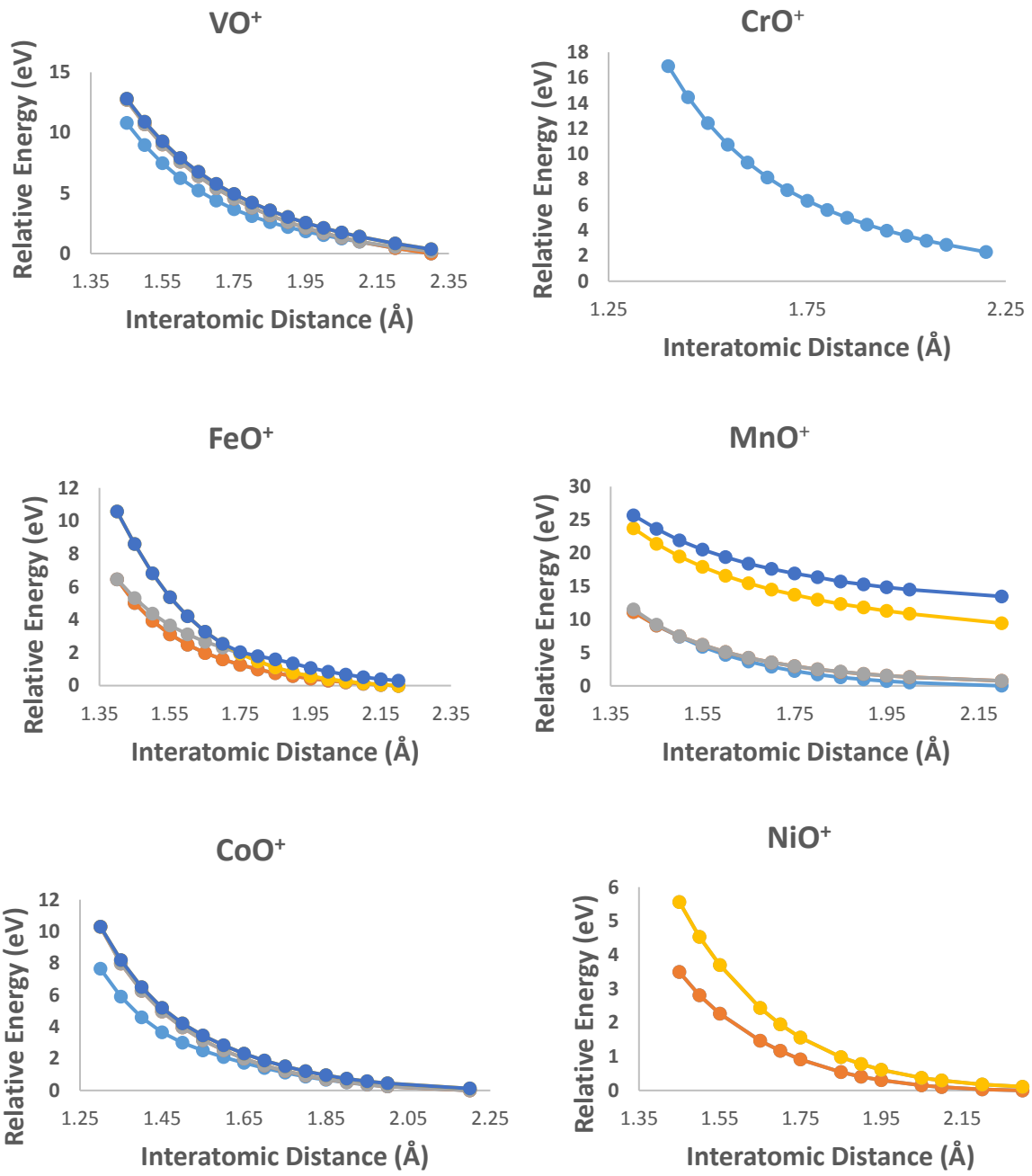

Figure 9: Complete active space potential energy surfaces for high spin cases.

Low Spin CAS potential energy surfaces

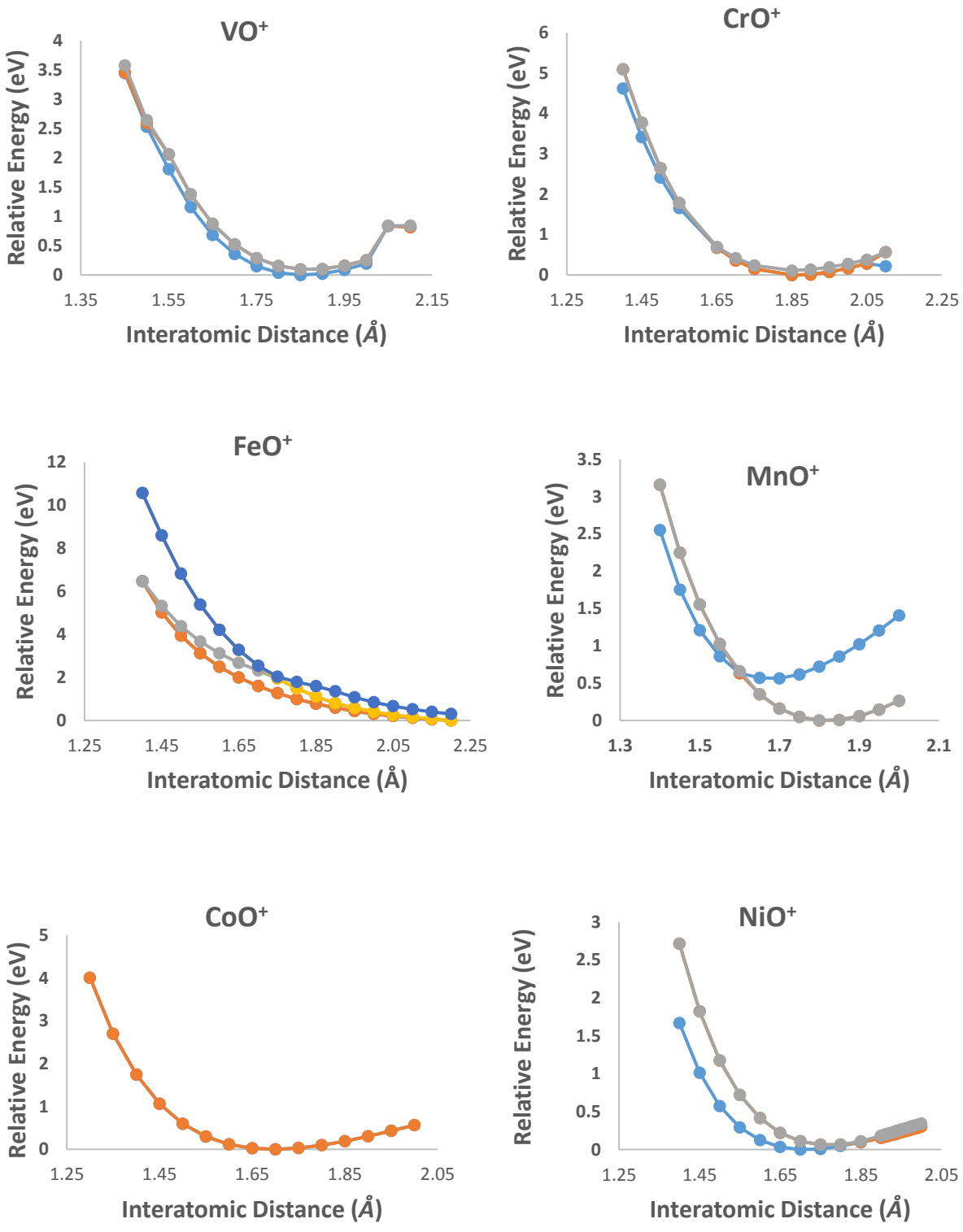

Figure 10: Complete active space potential energy surfaces for low spin cases.

Comparing the CAS calculations for the high spin and low spin cases, it is clear that high spin surfaces in general are repulsive, and do not show a minimum. Upon addition of electron correlation effects in MREOM, other low spin states are accessible. This should lead to finding bounded states. The low spin CASSCF do exhibit stable minima, except in the case of FeO^+. In the cases of VO^+ and CrO^+, degeneracies break down at the last point of the calculation. This would most likely lead to these geometries being excluded from the MREOM calculation.

3.5: Basics of Multi Reference Equation of Motion Calculations

Much like finding the appropriate CAS for a calculation, finding the right set of parameters to run a successful MREOM calculation can involve a good amount of trial and error. Unfortunately, MREOM calculations take significantly longer than CASSCF calculations. Each trial calculation runs for approximately one to three days, and the calculation is not guaranteed to be successful across the entire potential energy surface.

MREOM calculations are defined by the supplied CAS as well as the number of states requested. While it is possible to include the entire CASSCF calculation as a part of an MREOM calculation, it is preferable to separate them. This allows greater control and monitoring over the CASSCF calculation. Due to the size of the input file, the sample MREOM input file can be found in Appendix C. It is not necessary to understand every option of this input file, but important options will be detailed below. There are 3 main blocks of an MREOM calculation: the CASSCF, MRCI, and MDCI. The CASSCF block should exactly match the block found from the previous CASSCF calculation. Orbitals are read in from an Orca orbital (".gbw") file. The MRCI portion of the calculation is responsible for the calculation of T, S, X, D, and U amplitudes. The MDCI block is the final diagonalization of the resulting matrix whose eigenvalues give the requested energies. The most important parameters in the MRCI block are the 'STOL', 'DoSingularPT', and

'SingularPTThresh' options. Singular Perturbation Theory is a method for approximating T-amplitudes non-iteratively, and should be used as opposed to coupled cluster when issues involving T-amplitude convergence appear. Convergence issues in T-amplitudes at this point of the calculation are the main reason why an MREOM calculation might fail, and it is unclear at this time why certain calculations require this option while others do not.

In most cases, failing an MREOM calculation means that the supplied CAS wasn't of sufficient quality. This could be either due to discontinuities in the calculated potential energy surface, or due to issues with degeneracies in either the orbital occupancies or the calculated energy states. Occasionally, a CAS that looks perfectly converged may be passed to an MREOM calculation only to have that calculation fail. More than likely, the MREOM calculation would have failed calculating T and U amplitudes related to the transformation of the Hamiltonian. While most calculations may converge in less than 100 iterations, certain calculations such as VO^+ could be allowed 1000 iterations and still fail. These convergence issues are indicative of an issue calculating amplitudes related to the coupled cluster method, namely an issue with nearly singular equations.

From previous experience it is known that the solution of the cluster amplitudes in an MREOM calculation can be cumbersome. In regard to the calculated T Amplitudes (t_{ij}^{ab}) a tentative solution is available by replacing certain problem amplitudes by their first-order perturbative solution. The selection of such perturbative amplitudes is based on the eigenvalues of a suitable metric matrix. In practice there is a threshold to select [23]. This threshold is user selected and is based around the diagonalization of the metric matrices to obtain a set of orthonormal eigenvectors and eigenvalues, and discarding amplitudes related to eigenvalues below a certain threshold. However, simply discarding amplitudes can lead to jagged and discontinuous potential energy surfaces [23]. Replacing these amplitudes with a perturbative guess yields the greatest success. In general, one would like to select a threshold that just barely

encompasses the problem amplitudes. In ORCA, there is no simple way to accomplish this currently, so calculations must be tested by increasing the threshold iteratively. A clear issue with this procedure is that a different number of amplitudes may be replaced at different geometries, and that can lead to discontinuities in calculated potential energy surfaces. In the future, the threshold process may be replaced by an automatic threshold picking scheme, but this is outside the scope of this thesis [24].

The final block is the main part of the calculation, and where the program will spend most of its time. 'newblocks' are specified with a multiplicity as well as the number of states to calculate. This does not have to be the same as the states calculated in the CASSCF. While the MREOM calculation is sensitive to the supplied CAS, it is possible to calculate a CAS at a certain multiplicity and obtain a huge number of energies for different spin states. Every MREOM calculation has its associated quality checks. All cluster amplitudes T,S,X,D, and U should be relatively small, below about 0.10. IF they are large, 3 body contributions in the transformed Hamiltonian can be large, but are neglected. If some cluster amplitudes are large (0.1-0.15), the results from an MREOM calculation are questionable [23]. *Figure 11* shows an example of calculated T amplitudes.

```
      --------------------
      LARGEST T AMPLITUDES
      --------------------
16-> 22  -1-> -1       0.065483
16-> 29  -1-> -1       0.065321
18-> 47  -1-> -1       0.058644
17-> 46  -1-> -1       0.058644
18-> 35  -1-> -1       0.057465
17-> 34  -1-> -1       0.057465
16-> 33  -1-> -1       0.052265
16-> 42  -1-> -1       0.050569
11-> 29  -1-> -1       0.046262
18-> 40  -1-> -1       0.046074
17-> 39  -1-> -1       0.046074
16-> 30  -1-> -1       0.043835
18-> 21  -1-> -1       0.042248
17-> 20  -1-> -1       0.042248
11-> 42  -1-> -1       0.041957
18-> 28  -1-> -1       0.040540
```

Figure 11: Example T Amplitudes from a high spin CoO^+ MREOM Calculation. T amplitudes are well below the 0.1 calculation accuracy threshold.References weights from the final CI part of an MREOM calculation should be above 0.9. These reference weights are calculated for each state and are a measure of the CAS contribution in the final wave function. If this value is too low (<~0.90) then the accuracy of the resulting state is questionable. Unfortunately, passing these two checks does not necessarily result in a successful calculation. Curves could still have discontinuities or exhibit strange behavior. However, failing these checks removes any confidence that the results may be trusted.

3.6: MREOM Calculation Results and Discussion

The following are the completed potential energy surfaces from completed CASSCF calculations. In the following we will discuss MREOM calculations that start from the CASSCF results discussed before. While several CASSCF calculations can be completed in an hour, an MREOM calculation can take from 2 hours to 1 day. This meant that it takes a significantly higher time investment to find the correct settings

necessary for a successful MREOM calculation. In the following section, both the high spin and low spin results will be considered together and compared.

Table **9** includes details for each calculation.

Table 9: MREOM calculation details including number of states, multiplicities, elapsed calculation time, and SPT threshold.

	Basis Set	Multiplicity	Total States	SPT	Calculation Time
VO^+	ma-DKH-Def2-TZVP	9	N/A	No SPT	N/A (Failed)
CrO^+		10	39	0.01	7h46m
MnO^+		9	41	No SPT	2d22h
FeO^+		8	69	No SPT	10h55m
CoO^+		7	64	0.01	1d3h
NiO^+		6	91	No SPT	8h
VO^+		5,3	N/A	0.1	N/A (Failed)
CrO^+		4	39	0.1	3h19m
MnO^+		5	41	0.01	3h47m
FeO^+		6	69	0.1	11h15m
CoO^+		5	64	No SPT	1h51m
NiO^+		4	49	0.01	8h21m

Previously, theoretical and experimental studies have been conducted on the first series transition metal oxides for both neutral and charged species. A comprehensive study by Harrison et al. [25] was conducted on transition metal oxides for both neutral, cationic, and anionic species to calculate spectroscopic properties, such as vibrational frequencies and ground state spin states. Neutral species have also been investigated by Anderson et al. [26] and A. J. Merer [27], while charged species were studied by Fiedler et al. [28], Y. Nakao and K. Hiraro [29], Y. Shiota and K. Yoshizawa [30] to find ground state properties such as ionization energy or equilibrium ground state bond lengths for both neutral and charged species respectively. Approximate equilibrium bond lengths for the systems in this study are compared to both neutral and charged species in *Table 10*. Bond lengths used in this table are low spin

results that have been rounded to the nearest data point based on inspection of each curve. As such, this comparison is approximate, but shows a general agreeance within +/- 0.1 Å. To increase accuracy further comparisons require more points to be calculated near this equilibrium bond distance.

Table 10: Comparison of MREOM calculated bond lengths with literature for transition metal oxide cations

	Experimental Results	**Theoretical Results**							
Species	r_0 [27]	r_0 [25]	r_0 [26]	r_0 [27]	**Species**	r_0	r_0[28]	r_0[29]	r_0[30]
VO	1.59	1.60	1.55	1.59	**VO^+**	/	/	1.55	1.53
CrO	1.62	1.62	1.53	1.62	**CrO^+**	1.60	/	1.61	1.57
MnO	1.65	1.66	1.57	1.65	**MnO^+**	1.70	/	1.83	1.72
FeO	1.62	1.68	1.55	1.62	**FeO^+**	1.65	1.62	1.67	1.63
CoO	1.60	1.62	1.56	1.63	**CoO^+**	1.60	1.63	1.69	1.63
NiO	1.63	1.63	1.59	1.63	**NiO^+**	1.60	1.63	1.68	1.65

Please note that while it may appear that plots do not include the number of states listed above, all states have been accounted for. Several states are very close in energy and, depending on the range of states calculated, appear to overlap. While each calculation involves many states, it is a small subsection of the total number of states that exist for these potential energy surfaces. Attempting to calculate the entire potential energy surface is currently unfeasible.

3.6.1: MnO^+ Calculation and Discussion

Calculated MREOM potential energy surfaces are shown in *Figure 12*. The MnO^+ MREOM calculations have similarities, but differ due to jaggedness present in the high spin case. While the low spin case seems to have remained continuous, the high spin case involves some state mixing at around 1.70 Å to 1.80 Å. This occurs when the program calculates different states at different geometries. When setting up the calculation, the user does not decide to include specific states, but simply input several states per multiplicity. Problems occur if the program does not calculate the same states at each geometry. To assess the validity of each calculation, the reference weights and T amplitudes are examined for each geometry.

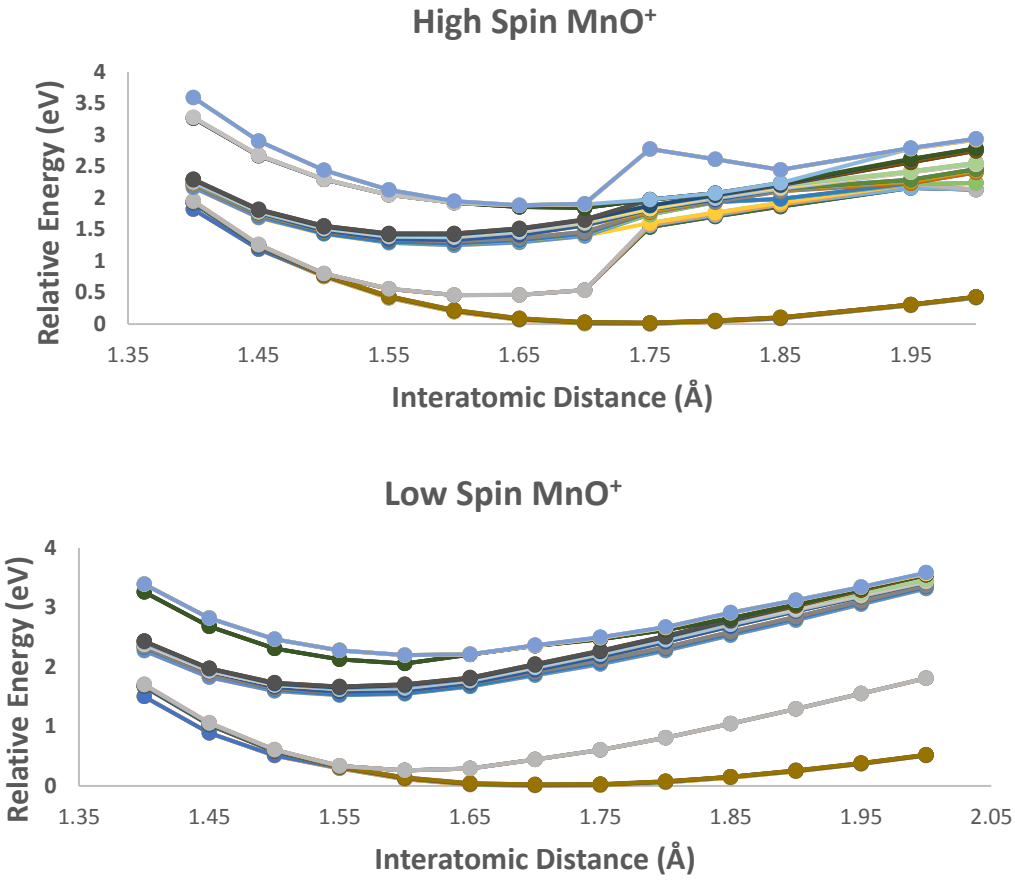

Figure 12: MREOM potential energy surface plots of MnO^+.

Table 11: Smallest references weights and largest T-amplitudes for high spin and low spin MnO^+.

Interatomic Distance (Å)	Smallest Reference Weights (High Spin)			Largest T Amplitudes (High Spin)		
1.4	0.8745	0.9036	0.9038	0.067779	0.06719	0.048935
1.45	0.8755	0.9053	0.9058	0.076563	0.060643	0.042937
1.5	0.8763	0.9066	0.9069	0.061426	0.048551	0.036614
1.55	0.8767	0.9051	0.9051	0.080213	0.077952	0.041718
1.6	0.8767	0.9033	0.9033	0.08842	0.086724	0.041006
1.65	0.8762	0.9016	0.9016	0.066612	0.06448	0.04143
1.7	0.8753	0.9	0.9	0.084372	0.045215	0.0403
1.75	0.8988	0.8988	0.9109	0.089201	0.057006	0.042703
1.8	0.8981	0.8981	0.9127	0.089327	0.084712	0.042571
1.85	0.8988	0.8999	0.9129	0.078069	0.076038	0.040513
1.95	0.9009	0.9019	0.9145	0.088258	0.086315	0.045744
2.0	0.9033	0.9041	0.9183	0.096399	0.093535	0.050526
Interatomic Distance (Å)	**Smallest Reference Weights (Low Spin)**			**Largest T Amplitudes (Low Spin)**		
1.4	0.9304	0.9304	0.9315	0.584819	0.584819	0.193995
1.45	0.9281	0.934	0.934	0.384476	0.384476	0.264742
1.5	0.9255	0.9382	0.9382	0.351814	0.237517	0.237517
1.55	0.9267	0.9424	0.9424	0.416985	0.161447	0.161447
1.6	0.9288	0.946	0.946	0.411187	0.120229	0.120229
1.65	0.9375	0.9473	0.9473	0.356044	0.095754	0.095754
1.7	0.9341	0.949	0.949	0.056244	0.054671	0.054671
1.75	0.9352	0.9487	0.9487	0.053831	0.049127	0.049127
1.8	0.9354	0.948	0.948	0.051837	0.045566	0.045566
1.85	0.9335	0.947	0.947	0.050214	0.049106	0.026308
1.9	0.9338	0.946	0.946	0.054304	0.048794	0.031118
1.95	0.9343	0.9433	0.9433	0.059901	0.047654	0.033962
2	0.9353	0.942	0.942	0.065933	0.046779	0.038823

After analyzing

Table 11, issues can be found with each calculation. Reference weights should stay above approximately ~0.90 and T amplitudes should not be higher than approximately ~0.1. For the high spin calculation, reference weights become small at low geometries, but become acceptable at r > 1.75 Å. For the low spin calculation, T amplitudes exceed the acceptable threshold for low interatomic distances, but become acceptable at 1.7 Å. This calls the first 0.4 Å of each calculation into question. To attempt to rectify this, the calculation was redone with a higher SPT threshold shown in *Figure 13*.

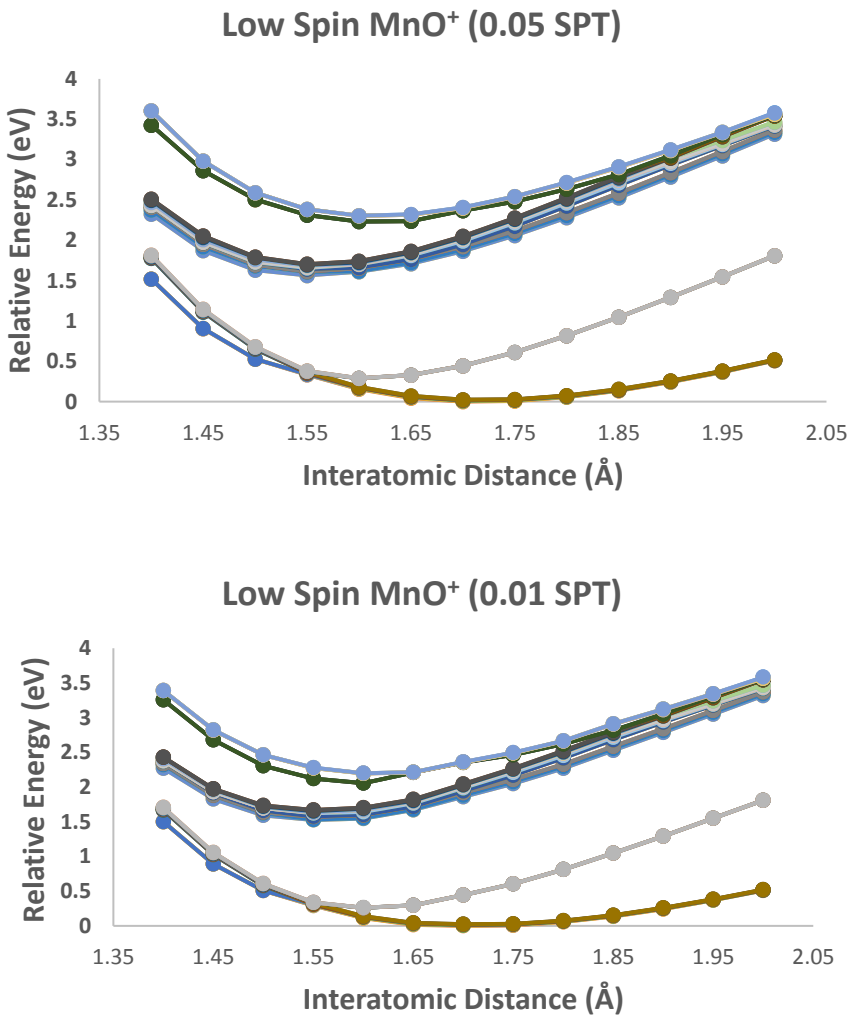

Figure 13: Comparison of SPT thresholds for low spin MnO^+. Increasing the SPT threshold had little effect on calculated energies but produced a large reduction of T Amplitudes as well as a slight increase in curve smoothness

The plots in *Figure 13* appear similar, with the higher SPT calculation appearing marginally less jagged. The main result of the increased threshold was that T amplitudes dropped significantly while results stayed largely the same. The calculation also completed faster, finishing in approximately three hours while the original calculation finished in four hours. From *Figure 14,* we can see increasing the SPT threshold had little effect on the calculation, but curves appeared less jagged.

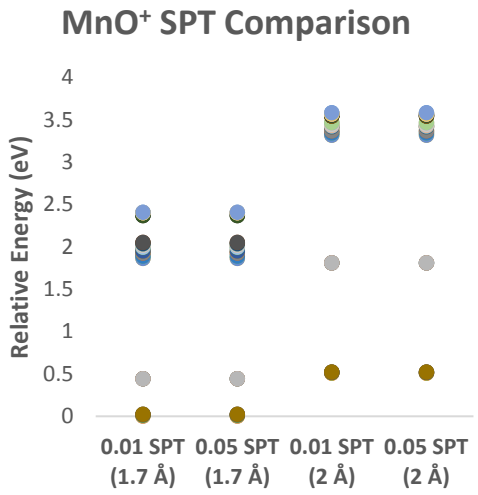

Figure 14: Comparison of energy values between differing SPT thresholds. Changing this threshold does not affect the calculated energies.

Table 12: Smallest references weights and largest T amplitudes for low spin MnO^+ with SPT=0.05.

Interatomic Distance (Å)	Smallest Reference Weights			Largest T Amplitudes		
1.4	0.9227	0.9377	0.9377	0.079	0.0286	0.0283
1.45	0.9244	0.9405	0.9405	0.0749	0.0281	0.0281
1.5	0.9271	0.9441	0.9441	0.0703	0.0268	0.0266
1.55	0.93	0.9481	0.9481	0.066	0.0276	0.0257
1.6	0.9327	0.9491	0.9491	0.0623	0.0282	0.0275
1.65	0.9346	0.9492	0.9492	0.0591	0.0318	0.0269
1.7	0.9332	0.949	0.949	0.0563	0.0356	0.026
1.75	0.9333	0.9485	0.9485	0.054	0.0398	0.0256
1.8	0.9334	0.9478	0.9478	0.0519	0.0443	0.0287
1.85	0.9335	0.947	0.947	0.0502	0.0491	0.0263
1.9	0.9338	0.946	0.946	0.0543	0.0488	0.0311
1.95	0.9343	0.9433	0.9433	0.0599	0.0477	0.034
2.0	0.9353	0.942	0.942	0.0659	0.0468	0.0388

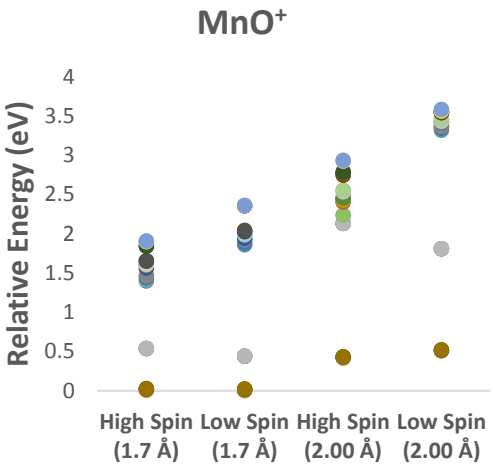

Figure 15: MnO^+ calculated energy comparison at two selected points.

Table 12 shows a promising result from raising the SPT threshold. Results now appear with reasonable T amplitudes and reference weights. Next, we compare calculated energy states in *Figure 15* between high and low spin calculations to see if the calculations show agreement. Each set of energies adheres to a similar pattern between calculations at 1.7 Å, while the calculations at 2.0 Å do not show agreement. The low spin case appears to be converging on an asymptote, while the high spin case does not. The midpoint calculations both show relative agreement, differing by about ~0.3 eV. This is surprising, due to potential issues with each calculation at that geometry. The general agreement between calculations lends these questionable sections some validity. From the above information, it appears that the high spin case trades a larger flexibility of calculable geometries for continuity errors in a section of the potential energy surface.

The low-spin calculations use a CASSCF reference that corresponds to the final states calculated in MREOM. The orbitals from such a CAS are better than orbitals from the high-spin CAS, and one would

expect low-spin results to be more accurate. The high-spin calculations are a bit of a stretch for the MREOM methodology and here we explore the ability of MREOM to recover from poor starting orbitals.

3.6.2: FeO^+ Calculation and Discussion

From *Figure 16*, we can see several irregularities in the low spin plot, and a few in the high spin plot over the course of the calculation. The high spin calculation was able to be completed up to 6.0 Å, but results were poor past 2 Å. T amplitudes were not converged for r > 2 Å for the low spin case. While both potential energy surfaces have a degree of strangeness to them, the high spin case appears more continuous than the low spin case. From this point on, T amplitudes and reference weights can be found in Appendix D.

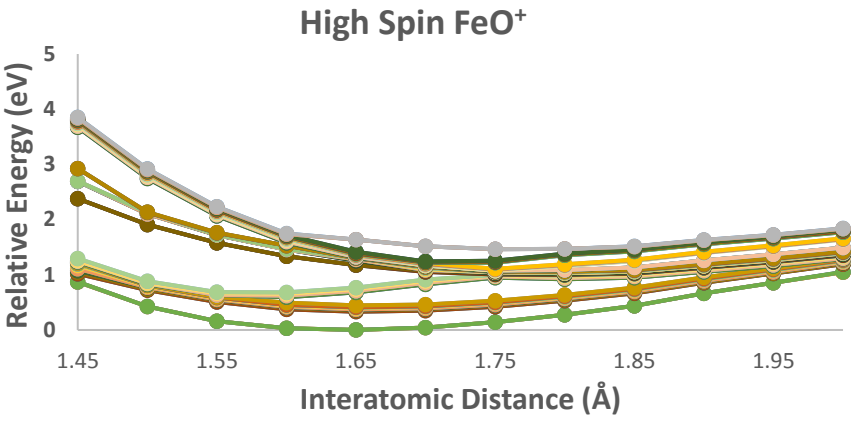

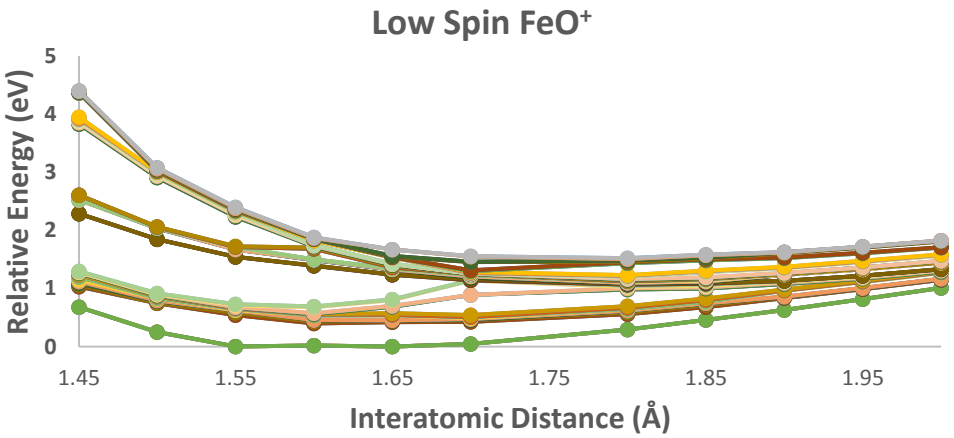

Figure 16: MREOM potential energy surface plots of FeO^+. The high spin method (top panel) produces a less jagged curve compared to the low spin method (bottom panel) for this system.

In general, both quality indicators appear satisfactory. However, the high spin case borders on questionable, with T amplitudes and reference weights both approaching unsatisfactory values. In the low spin case, reference weights start a bit low but quickly grow. T amplitudes begin small and grow slightly, but stay reasonable throughout the entire calculation. From the energy comparison in *Figure 17*, both calculations appear to agree on the energy range where states occur, but not on the distribution of states within that range. In this calculation, the high spin case appears more continuous and well behaved when compared to the low spin calculation and is the preferred calculation for this system.

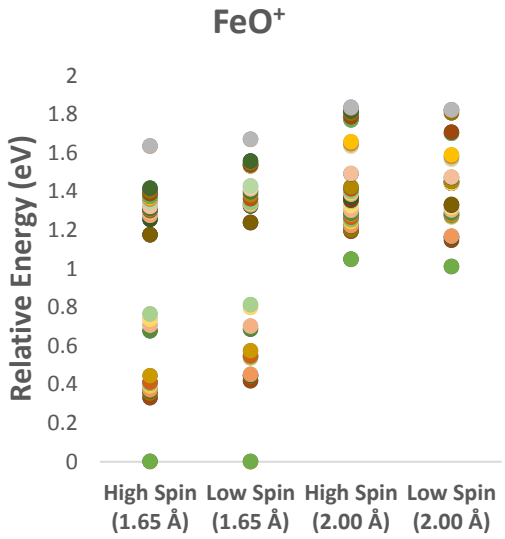

Figure 17: FeO^+ calculated energy comparison between spin cases.

3.6.3: CoO^+ Calculation and Discussion

Figure 18 shows the results of the MREOM calculation using each spin approach for CoO^+. The high spin and low spin systems exhibit the same properties that occurred in previous calculations. The high spin calculation allows convergence for a greater range of geometries than the low spin case, while exhibiting jaggedness around 1.9 Å and state mixing past 1.8 Å. There are no obvious discontinuities in the low spin calculation. Appendix D contains reference weights and T amplitudes for the above surfaces.

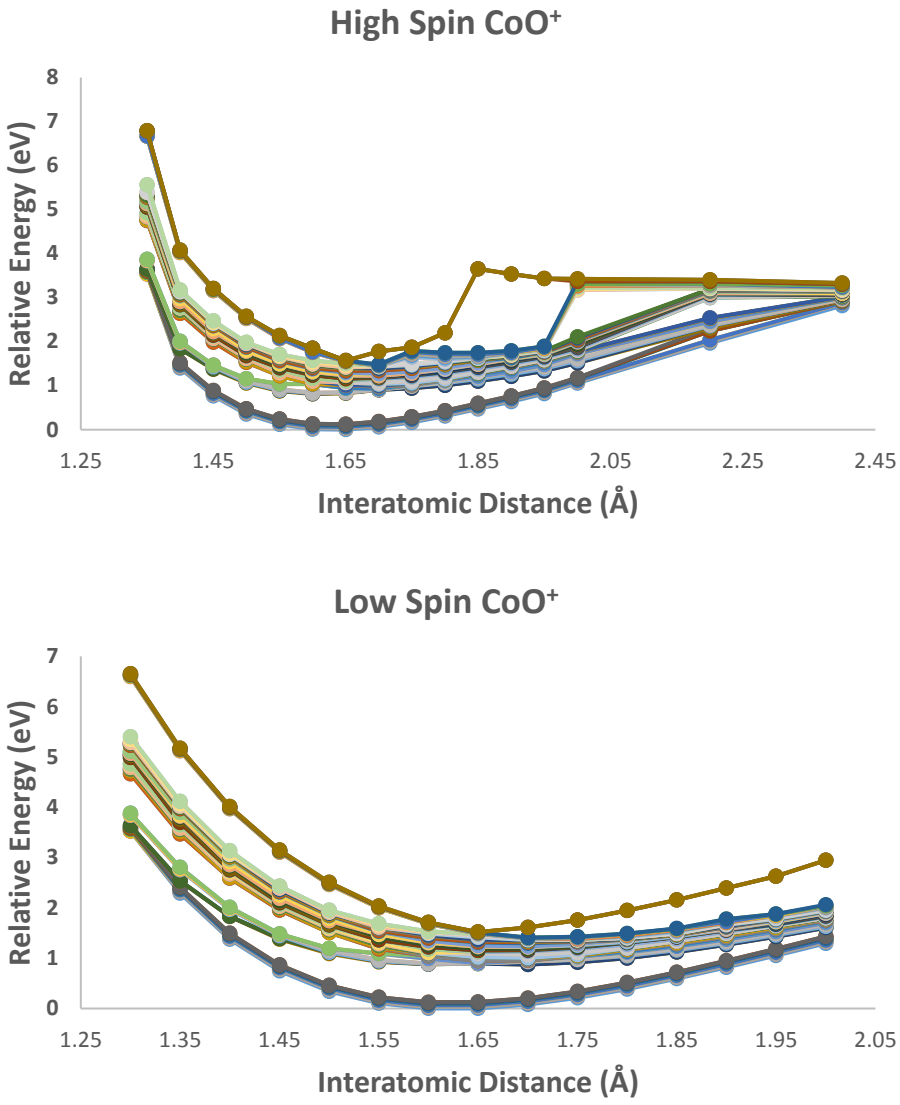

Figure 18: MREOM potential energy surface plots of CoO^+.

Reference weights and T amplitudes are satisfactory. In the high spin case, reference weights are at their lowest but still above acceptable standards. This does not explain the discontinuities found in the high spin case above 2Å. This is once again most likely due to state mixing, with calculations picking up separate states at different geometries, which converge on the same asymptote as geometries approach complete separation. However, upon visual inspection of both potential energy surfaces, the high spin

system PECs are more jagged than those of the low spin system. The curves produced by the low spin MREOM calculation appear to be reasonable.

3.6.4 NiO^+ Calculation and Discussion

Figure 19 shows the results of the MREOM calculations for NiO^+. Once again, the high spin case was able to calculate a larger range of geometries for the potential energy surface. However, the high spin case includes significantly more jagged curves, with many curves showing a jump of about ~1 eV. This jump is not observed in the low spin case. Note that the high spin case includes an extra 42 states. These were included to account for the jaggedness by attempting to remove the state mixing issue. Appendix D contains T amplitudes and reference weights for the above calculations.

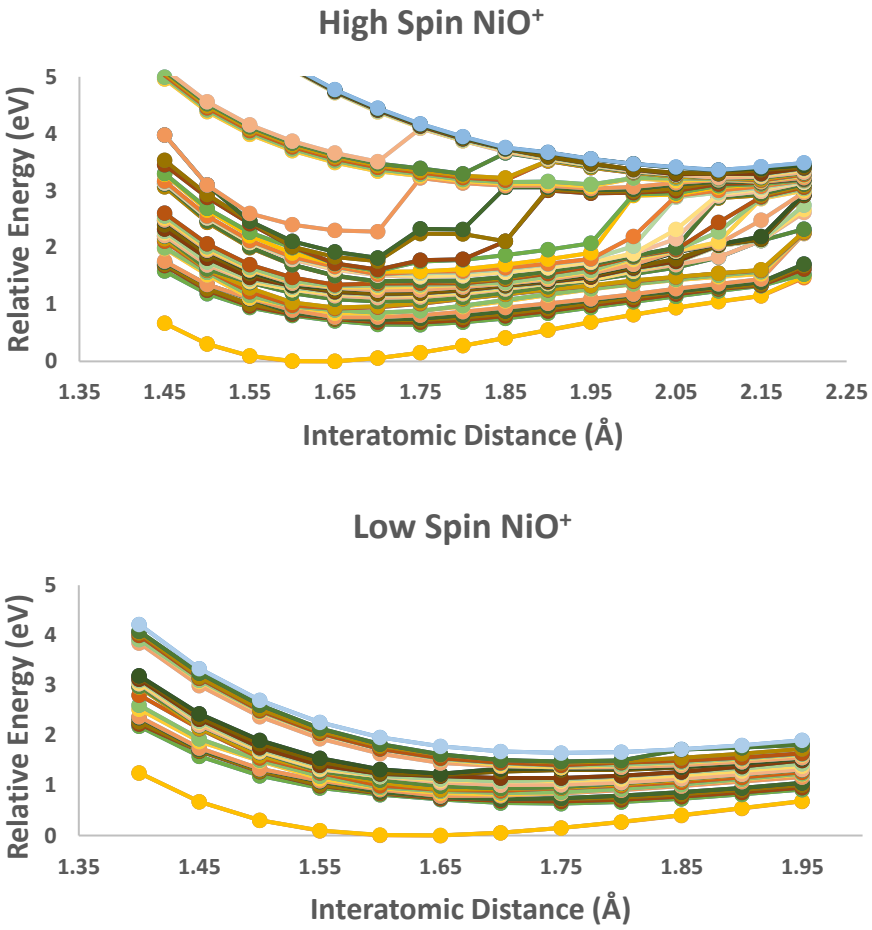

Figure 19: MREOM potential energy surface plots of NiO^+. Here we see significant discontinuities in the high spin calculation, including state-mixing along the potential energy curves for higher energy states.

For the high spin case, T amplitudes and reference weights are both approaching thresholds suggesting that certain states may not be accurate. As explained previously, extra states were included in the high spin calculation, which are meant to be removed to create a continuous and well-behaved potential energy surface. *Figure 20* is the result of the edited high spin surface:

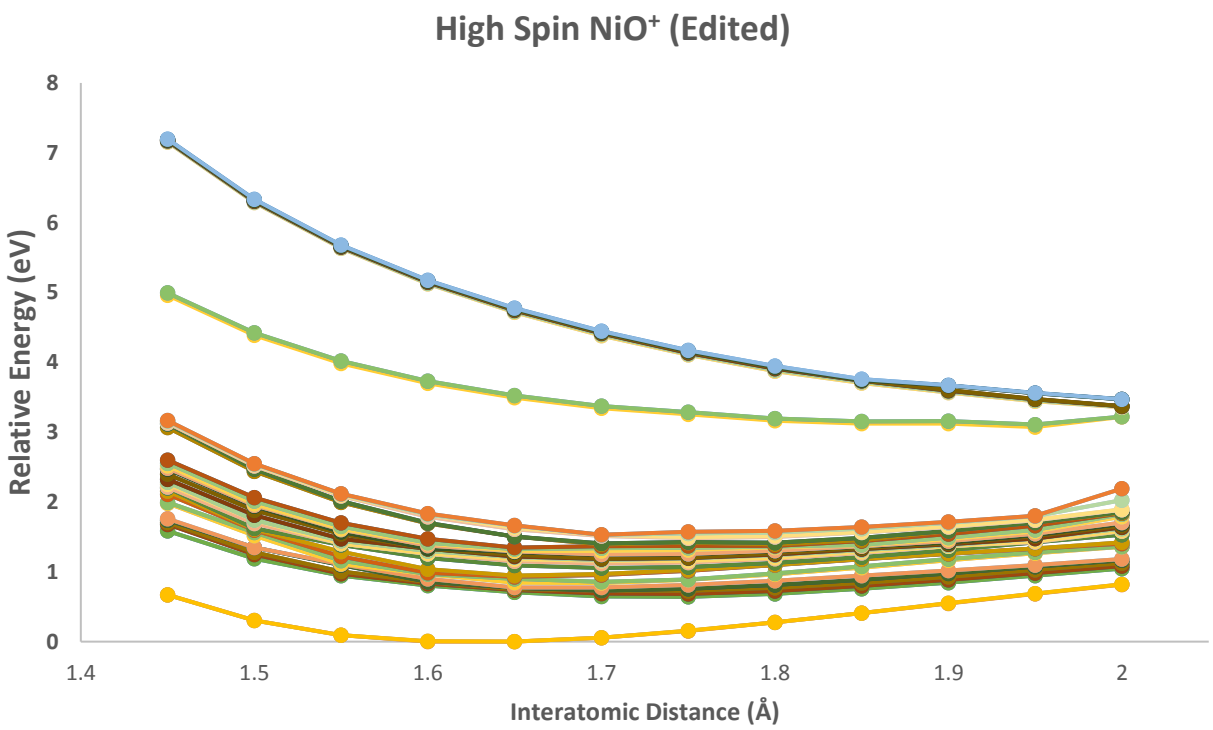

Figure 20: Edited high spin NiO^+ potential energy surface. Curves that were discontinuous have been removed.

To compare plots easily with the low spin case, the high spin cases' surface was truncated after removing the jagged curves. The two plots begin to appear similar, but more analysis is required. *Figure 21* is a comparison of calculated energy states at two separate points. This state energy plot shows general agreement between the high spin and low spin calculated plots after editing the plots to remove jaggedness. Each exhibits a similar gap of about ~0.8 eV for the first energy level gap, leading to a dense cluster of states. While the two plots are very similar, the high spin case was significantly easier to set up on the CAS level, with the MREOM calculation completed along more or less the same timeline. One of

the main strengths of MREOM is its ability to calculate many states simultaneously. This makes the impact of requiring extra states needed to make an accurate high spin plot negligible. The above strategy allows for high spin MREOM calculations to create continuous potential energy surfaces for complicated electronic systems.

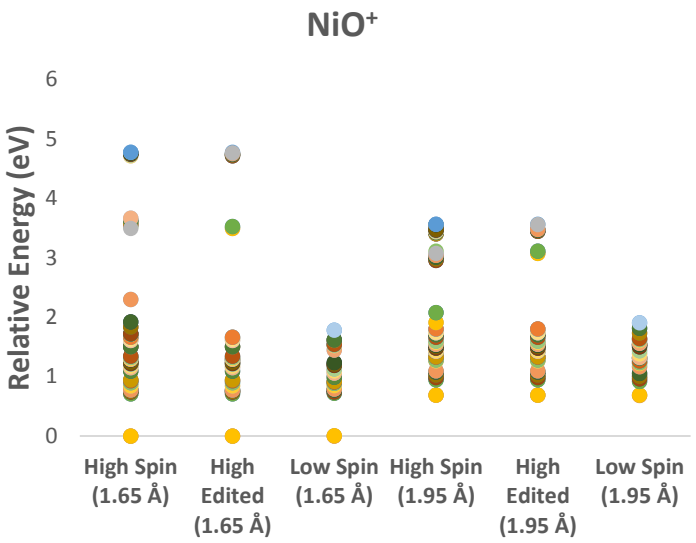

Figure 21: NiO^+ calculated energy comparison. There is good agreement between the edited high spin and low spin calculations.

3.6.5 CrO^+ Calculation and Discussion

The plots of CrO^+ found in *Figure 22* are an interesting case in this study. For the other transition metal oxides, the high spin potential energy surface appeared with jaggedness and discontinuity between the midpoint and asymptote, but were stable across a much larger range of geometries. The low spin case would have a smaller range, but curves would be smoother. Here, the high spin curve appears significantly smoother than the low spin case, while still enjoying the benefits of a much more stable CAS. Once again, appendix D contains reference weights and T amplitude data. From Appendix D, some trouble reference weights and odd T amplitudes are found for both the high spin and low spin cases.

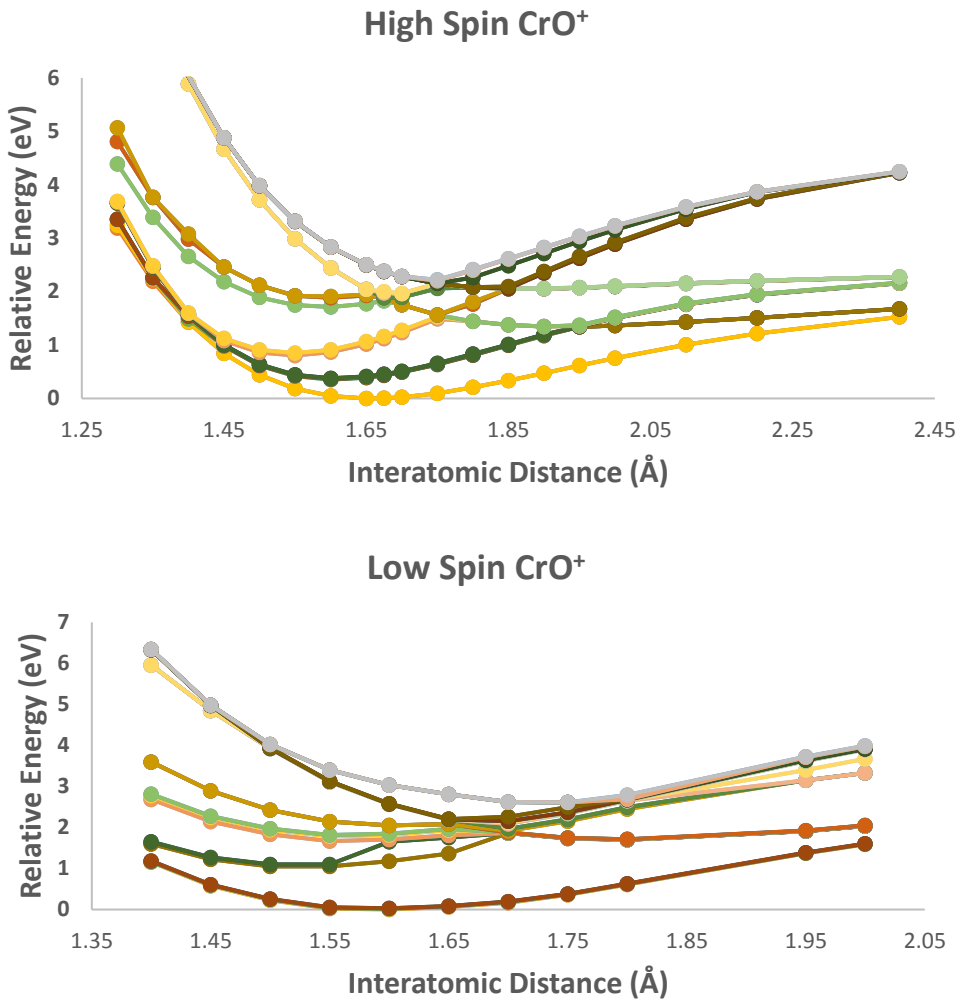

Figure 22: MREOM potential energy surface plots of CrO^+.

For the high spin case, something odd occurs in the T amplitudes at 1.55 Å and 1.65 Å. While reference weights of all the included states stay high, the T amplitudes of those points calls into question the calculated energies. Despite how the high spin calculation looks, results appear questionable due to the low reference weights for several states at most geometries. When we compare energy states between calculations in *Figure 23*, results do not line up.

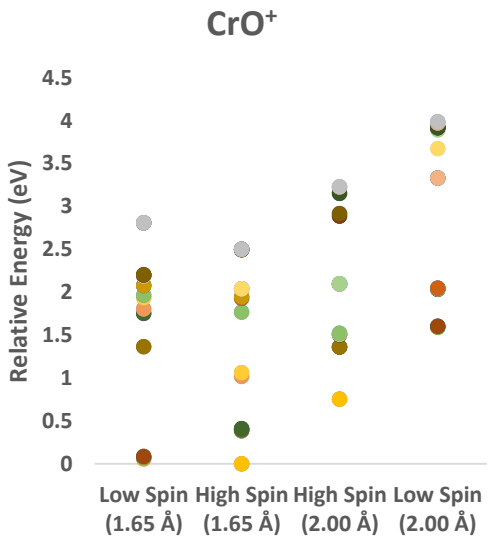

Figure 23: CrO^+ calculated energy comparison.

Here, we see little agreement between the two calculations. Gaps between states do not line up between calculations. For the midpoint case, the only energies that appear to agree are the cluster of energies around ~2eV. For the endpoint case, calculations have a similar pattern but disagree on both the highest and lowest state. Overall, there is a very weak agreement between the calculations that does not inspire confidence. In this case, the high spin calculation appears preferable despite the low reference weights for a handful of states at each geometry. However, T amplitudes stay low throughout the calculation. Despite low reference weights, curves remained continuous and appear without any irregularities. The high spin calculation for CrO^+ appears trustworthy. CrO^+ is the only system in this study where the high spin case appeared well behaved without editing out states, compared to the discontinuous curves calculated for each other system.

3.6.6 VO^+ Calculation and Discussion

Unfortunately, an MREOM calculation for VO^+ was not completed for any of the several CAS configurations attempted. Both high and low spin were attempted, as well as a mixed spin CAS calculating states from several multiplicities. In some cases, a CAS would not remain stable across the entire range of

geometries. Mixed spin active spaces are more complicated to converge, with high spin cases being the simplest to both create and converge. This was the reasoning behind using the high spin regime in the first place. Most calculations failed in the T amplitude stage. *Table 12* denotes the results of each MREOM calculation involving VO^+. Each MREOM calculation that was able to run did so at 1000 iterations. Note that most other calculations converged before 100 iterations, with only one calculation requiring 230. In contrast, the calculations for VO^+ were more resistant toward converging T amplitudes than other calculations. The tolerance for T amplitude convergence is 10^{-6}.

Table 13: MREOM results for VO^+.For each CAS that converged, MREOM calculations were conducted. The T amplitude residual was not able to be converged sufficiently to complete the calculation.

Electrons	Orbitals	Multiplicity	States	CAS Convergence?	T Amplitude Residual
8	8	3	3	No	N/A
8	9	3,1	5,5	No	N/A
8	9	5	3	No	N/A
8	8	5	3	No	N/A
8	8	3,1	5,3	Yes	Running
8	8	3	1	Yes	0.010126407
8	8	3,1	5,5	Yes	0.002531189
8	9	5,3,1	2,3,3	Yes	0.000931845
8	9	9	5	Yes	0.000066
6	7	5	3	Yes	0.000022599

From the above, it appears that the CAS involving the fewest states resulted in the slowest convergence. However, the active spaces that involved many state from several orbitals were also slow to converge, fairing only slightly better. The CAS that was closest to convergence involved the fewest orbitals, removing two due to problems with orbital occupancy. The increased convergence could simply be due to involving fewer orbitals as opposed to finding the correct CAS. As of this writing, other CAS configurations are being attempted. As current calculations have not come close to proper convergence,

it is unclear what CAS configuration might yield suitable results. In the end, none of the attempted calculations yielded anything suitable.

3.7: Conclusion

In this study, six transition metal oxide cations were examined using MREOM: VO^+, CrO^+, MnO^+, FeO^+, CoO^+, NiO^+. These systems were approached using two different spin regimes; a high spin regime created to simplify the CAS process, and a low spin regime used as a more sensible approach. VO^+ was additionally approached with a mixed spin CAS when other approaches failed, but did not yield a potential energy surface. From the five systems that were completed, the low spin case was the more reasonable calculation in three of the five calculations, with FeO^+ and CrO^+ appearing to behave better as high spin calculations. This is interesting, as the idea that high energy high spin states can be used as a reference to calculate states significantly lower in energy is unintuitive. However, it is unclear how accurate these calculations are due to high T amplitudes and sub-optimal reference weights.

For MnO^+, CoO^+, and NiO^+, results were significantly better behaved in the low spin case when compared to the high spin case. Curves appeared continuous with low T amplitudes and high reference weights. The only issue with these calculations was the difficulty in setting them up. Originally, the high spin regime was introduced to simplify the CAS selection process. Unfortunately, the high spin case failed for two of the above systems due to issues with convergence of T amplitudes. This might be solved with a more aggressive approach to choosing a singular PT threshold, as it is theorized that issues with T amplitudes or jaggedness could be due to different numbers of amplitudes being frozen depending on the current geometry. Currently, there is no way to choose a fixed number of T-amplitudes to approximate.

Unfortunately, even when allowed more than three times the iterations of the other calculations, it was not possible to converge T-amplitudes for either spin regime of VO^+. This might be explained by the increased density of states of V^+ compared with the other transition metals, requiring a larger CAS to

properly calculate a potential energy surface. As these states begin to converge asymptotically, calculating these states becomes significantly more complex.

While the high spin results involved discontinuities, these discontinuities could be addressed in NiO^+ by calculating many states and trimming down until only continuous curves remain. Using a high spin CAS is not an intuitive response to convergence issues, as the states included in the CAS are often very far from the ground state of the system. By editing the high spin NiO^+ plot, a continuous and well behaved potential energy surface was obtained. While this strategy may make the high spin approach viable, it is unclear if this produces sufficiently accurate potential energy surfaces. While NiO^+ could be edited to show general agreement, the other systems showed disagreement between calculation regimes. In the case of CrO^+, high T amplitudes and low reference weights make the results appear questionable.

In this chapter a high spin and low spin calculation approach was applied to six systems, with five systems viable potential energy surfaces. While the high spin case was significantly easier to set up, the low spin case calculated smoother curves for three of the systems in this study. While the cost of running a high spin calculation is generally low for the user, the calculations take longer to finish and results appear questionable. By editing the high spin curves, it was possible to add extra states for later removal to create a smoother potential energy surface. In the end, the low spin case yielded several reasonable potential energy surfaces and is recommended. However, the unintuitive high spin approach with editing may also be considered as a simple to run alternative.

The goal to calculate many potential energy surfaces for complicated transition metal oxides is ambitious. A clear alternative to MREOM is to use MRCI calculations. This would require a large state-averaged CAS calculation, and this might compromise the accuracy of the calculation. MREOM is designed to have fewer issues in this regard, but as evidenced from the current work the MREOM approach can suffer from numerical instabilities. The use of symmetry in the calculations might alleviate some of the

problems, and certainly would allow for a better targeting of states. However, this would require a major re-implementation in ORCA. These studies show that MREOM calculations are not sufficiently robust to calculate full potential energy surfaces. MREOM can be used to calculate single point energies, and one might calculate several single point energies at close lying geometries to extract a low-order Taylor series expansion. In the future this can be expanded to calculate parameters for non-adiabatic vibronic models. [25]

Chapter 4

New Method for Implementing MREOM

In the first chapter of this thesis the basics for an MREOM calculation was established, as well as the theory behind MREOM. Similarity transformations are applied to a bare Hamiltonian H such that excitations out of the CAS are removed. These transformations do not effect the eigenvalues of the Hamiltonian, meaning that transforming the Hamiltonian does not change the energy levels. In this chapter, an algorithm will be introduced to create a new CI program designed to perform MREOM calculations. This program is meant to take advantage of the efficiency of heavily optimized common use linear algebra libraries. A data structure was created such that arrays could be easily passed to these linear algebra subroutines. This would allow efficient calculation of several integrals at once while avoiding the array reshuffling present in current implementations of MREOM.

Unfortunately, this project was not completed. The CI Code was meant to be completed on ASUS2 using FORTRAN, which would later be ported to C for ORCA. The ASUS2 version of the code was meant to be a proof of concept, with practical calculations using ORCA. The main advantage for calculations run using ORCA is the inclusion of spin-orbit coupling, which increases the accuracy of the calculation by accounting for energy level shifts due to the interaction between an electron's spin and orbital motion. In the end it was deemed too much investment to get the program running on ACES2 to just immediately port it to ORCA for actual use. This code will most likely be completed by a future student in ORCA.

The algorithm being implemented in this study is a Davidson Algorithm. The heart of the algorithm is to use preconditioners to create a guess input vector $|\varphi\rangle$. The next step is to then construct a representation of the Hamiltonian **H** from these guess vectors:

$$H_{pq} = \langle \varphi_p | \hat{g} | \varphi_q \rangle \tag{16}$$

Next, we diagonalize this Hamiltonian:

$$\boldsymbol{H C_p} = E \boldsymbol{C_p} \tag{17}$$

Then calculate the current best estimate:

$$|\psi\rangle = \sum_{p=1}^{N} |\phi_p\rangle C_p \tag{18}$$

Next the residual is calculated:

$$Rk = \langle Xk | \hat{g} - E | \psi \rangle \tag{19}$$

If the residual is above some tolerance value, then new guess vectors are calculated:

$$\varphi = (H_0 - E)^{-1} Rk \tag{20}$$

With the process repeated from the 2nd step until the calculation converges. While both the current implementation of MREOM and the proposed implementation use a Davidson algorithm, they are implemented in different ways. The heart of the matter is that improvements can be made to the efficiency of the current CI program.

Table 14 shows the percentage of time spent in each part of an MREOM calculation for a variety of systems. The most time-consuming step was found to be final matrix diagonalization.

Table 14: Relative timings of each calculation section for MREOM calculations in ORCA.

System	CASSCF Iterations	MDCI Module	MRCI Module
NiO^+	0.001	0.314	0.685
MnO^+	<0.1%	0.036	0.963
FeO^+	0.001	0.102	0.897
CoO^+	0.001	0.257	0.742
CrO^+	0.008	0.434	0.559

From *Table 13*, we can see that the program spends most of its time in two separate CI portions, both dedicated to matrix diagonalizations. The current implementation of the MRCI code is a generalized non-specific algorithm designed to treat one integral at a time. A new algorithm was developed with a unique data structure in mind such that multiple integrals could be processed in a single matrix-matrix multiplication call. This data structure is shown in *Figure 24.*

CAS	C(n, λ)
1h	C(i, n, λ)
1p	C(a, n, λ)
1h1p	C(a, i, n, λ)

Figure 24: Data structure used in the new algorithm. This data structure would allow for the intelligent storage of our data, with 'simpler' indices treated later by the different loops of the program.

The orbital labels, i and a, refer to inactive low energy hole orbitals that are doubly occupied in each reference determinant and virtual orbitals that are empty in the reference state. In MREOM calculations we are often interested in many electron states. States which have the same spatial symmetry represented by irreducible representations and spin values, namely the S_z and S^2 values, can share the same data structure. The individual sates are categorized by the index n. These states can all be treated together in a block Davidson algorithm. The matrix multiplication of **HC** is carried out for a block of states all at once and is shown in *Figure 25*. The most complicated label to use is the occupation string of orbitals

in the active space. This string is indicated by the Greek indices (λ, μ, etc.) and represents the active space character of the contribution. Each string is characterized by irrep, number of electrons, and S_z value, with all possible strings occurring consecutively.

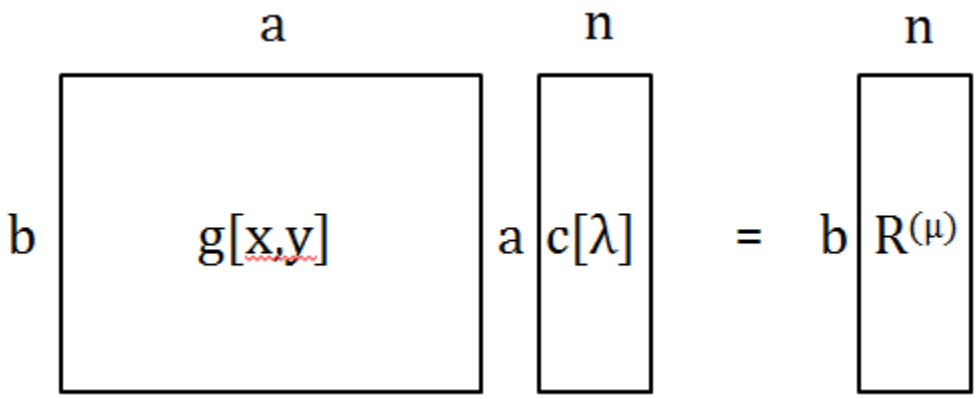

Figure 25: Structure of a matrix-matrix multiplication. Much of the algorithm depends on exploiting matrix-matrix multiplication calls.

While this algorithm is more efficient, it is significantly more complicated. Each contribution requires a specialized and unique loop structure. While the current implementation spends a significant amount of time diagonalizing matrices, it has a 'one size fits all' solution. This means that while the new algorithm would be much faster, development time would both be significantly longer as well as more complicated. Due to the nature of calculations in quantum chemistry requiring testing many different systems a streamlined and efficient CI code is required to push the state of the art forward.

Each contribution must be individually calculated for both the one electron and two electron contributions. This means that some residual **R** is calculated by multiplying our Hamiltonian **H** with some input vector **C**, for both the one electron and two electron cases. Examples of this multiplication can be seen below for each case:

$$R_{n\mu} = -\Sigma_{x,i,n,\lambda}\, h_{ix}\langle u|x|\lambda\rangle C_{in\lambda} \tag{21}$$

$$R_{n\mu} = -\Sigma_{k,x,y,z,n,\lambda} \langle kx||zy\rangle\langle u|x^{\dagger}yz|\lambda\rangle C_{k\lambda} \quad (22)$$

Equation 22 shows a one electron example, where Equation 23 shows a two-electron example. Labels *i,j,k* refer to hole electrons, whereas *x,y,z* refer to active space electrons. As mentioned in Chapter 1, all 1h, 1p, 1h1p, and 2h contributions are determined and calculated. This is done by determining each valid residual contribution and finding what combination of Hamiltonian and **C** vector labels determines this residual. Determining each contribution involves engineering a Hamiltonian and **C** vector pair whose multiplication results in a particular residual. Contributions that result in residuals with the wrong electron character are discarded. In each of the above cases, the sum labels give an idea of what labels will be looped over in the code.

Each matrix is designed to be stored in memory consecutively as per the data structure stated previously, with less complicated labels appearing first and more complicated labels appearing second. This means that every contribution has a calculable starting point and end-point determined by the properties of the system being looked at. In truth, the program stores the entire array in memory and determines what pieces need to be used by a particular subroutine by calculating a series of 'offsets' during the initiation of the program. These offsets are stored and are used by a pointer to determine how to correctly access relevant parts of the residual, Hamiltonian, and CI vectors. This is visualized in *Figure 26*.

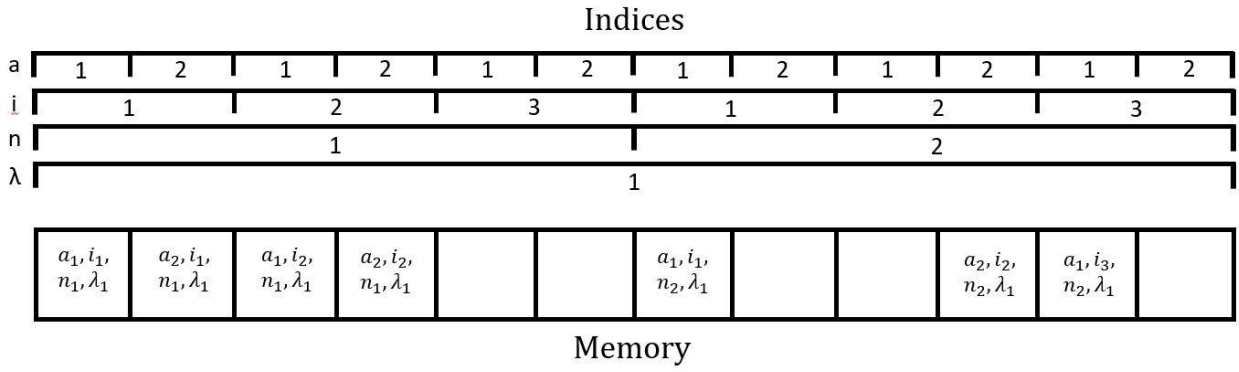

Figure 26: Example of array in memory. The nature of the data structure and each element appearing consecutively in memory allows matrix-matrix multiplication calls to be exploited for massive gains in efficiency.

Depending on what contribution is being looked at, several integrals can be calculated simultaneously with a single matrix-matrix multiplication call. For example, the contribution shown in Equation 23 may be looped simply, While the contribution found in Equation 24 must be looped over explicitly due to its complexity:

$$R_{n\lambda} = +\Sigma_{i,a,\lambda}\, h_{ia}\langle u|\lambda\rangle C_{ain\lambda} \tag{23}$$

$$R_{inu} = +\Sigma_{x,i,j,k,\lambda}\, h_{jx}\langle u|x|\lambda\rangle C_{ijn\lambda} \tag{24}$$

Put simply, the complexity of a contribution is determined by how, if possible, different labels may be 'glued' together. For example, the first contribution is made possible by gluing together the 'a' and 'i' labels. Since no active space electrons occur, the active space in both the input vector and residual remain identical, and so the final two labels may also be glued together. This results in the following pseudo-code:

$$R(1, n\cdot\lambda) = sum(i,a)H(1, i\cdot a)\times C(i\cdot a, n\cdot\lambda) \tag{25}$$

Whereas the second example is more complicated due to the inclusion of an active space electron. Each time an active space electron is involved, a subroutine must be called to calculate how the active space electron operates on the original active space string to determine a new active space string. Most contributions require an active space electron, but most contributions can also be simplified in some way. The pseudo-code from equation 4 can be found rewritten below:

$$R(i\cdot n, \mu) = sum(i)\times V(1, j)\times C(i, j; n, \lambda)^T \tag{26}$$

Where the 'T' denotes a transposed array. This is required due to a mismatch of labels between the Hamiltonian and the input vector and the residual. What this means is that each active space and state

label must be looped over explicitly, and within that loop each C(i,j) matrix used must be transposed before being multiplied with the Hamiltonian. Since each loop must be treated explicitly, this contribution requires more time to complete. A full list of contributions, along with the pseudocode associated with each contribution, can be found in appendix A.

As stated previously, one of the main benefits of writing this algorithm and data structure is the ease and efficiency of matrix-matrix multiplication using the Basic Linear Algebra Subroutines (BLAS) library. This library has been heavily optimized to provide extremely efficient linear algebra functions. Taking proper advantage of these already-optimized subroutines allows for a large speedup in the CI code. The backbone of the code comes from structuring our contributions such that we make as few calls using BLAS as possible, as each call will still be the bottleneck of a calculation.

The following will be two pseudo-code examples of subroutines in the CI code; the first will be a one body Hamiltonian contribution and the second will be a two-body contribution. The two-body contribution is more complicated, but most of the complication comes from proper configuration of arrays, offsets, and labels to correctly determine each contribution.

4.1 Code example of one body Hamiltonian

We will start by looking at the contribution from before, shown in equation (3). Equation 28 shows both the equation form and pseudocode form of this contribution. This contribution is simple compared to other one body contributions. There are no active space contributions, which means that the active space label found in the input array is the same as the label in the residual. This means that the active space and state label may be looped over simultaneously. The form of the residual and the form of the input vector also means that the hole and particle labels 'a' and 'i' can also be looped over simultaneously. This will be addressed in the way that the matrix-matrix multiplication is set up at the end of the subroutine. First, the code will be written in its entirety on the following page. Then, each section will be analyzed.

$$R_{n\lambda} = +\Sigma_{i,a,\lambda}\, h_{ia}\langle u|\lambda\rangle C_{ain\lambda} \tag{27}$$

$$\mathrm{R}(1, \mathrm{n}\cdot\lambda) = \mathrm{sum}(\mathrm{i},\mathrm{a}) \times \mathrm{V}(1, \mathrm{i}\cdot\mathrm{a}) \cdot \mathrm{C}(\mathrm{i}\cdot\mathrm{a}, \mathrm{n}\cdot\lambda)$$

```
do aspin=1,2

     do arep=1, nirrep
          ispin = aspin
          irep = arep

          ni = js_norb(o_h, irep)
          na = js_norb(o_p, arep)

          s_C = s_ph(aspin,ispin)
          s_R = s_0

          ioff = js_orb_offh(irep,ispin) -1
          aoff = js_orb_offp(arep,aspin) -1

          nlambda = js_nactive(s_C)

          do a = 1,na
               do i = 1,ni
                  v2(a,i) = hmat(ioff+i,aoff+a)

          C_start = js_off_psi(s_C, arep, irep)
          R_start = js_off_psi(s_R, 1, 1)
```

```
 nsum = na*ni
 nrow = 1
 ncol = nstate*nlambda
 fact = 1.0d0

Call matrix-matrix multiplication
(nrow, ncol, nsum, fact,
 v2, maxorb,
 C(C_start), nsum,
 R(R_start), nrow)
```

At this time, portions of the code will be individual examined. The program begins with the following code snippet:

```
do aspin=1,2
     do arep=1, nirrep
          ispin = aspin
          irep = arep
```

Each spin and irreducible representation must be explicitly looped over, so that every contribution is accounted for. In this case, the spins and irrep between the 'a' and 'i' particles are identical. This is a corollary of how this particular contribution was derived. In most cases, the spins of the particles must be the same such that the state is not annihilated as per the rules of second quantization. In the above, the code starts at 1 and ends at 2 for the spin loop, and loops several times equal to 'nirrep' for the irreducible representation loop. 'nirrep' is one of the many variables that is initialized by the program during startup based on the system in question.

```
ni = js_norb(o_h, irep)
na = js_norb(o_p, arep)

s_C = s_ph(aspin,ispin)
s_R = s_0

ioff = js_orb_offh(irep,ispin) - 1
aoff = js_orb_offp(arep,aspin) - 1

nlambda = js_nactive(s_C)
```

Here is where the many different offsets are calculated. 'ni' and 'na' refer to the number of orbitals related to that set of electrons, based on the character of that set (hole, particle, active) and what representation is being currently looked at. 's_C' and 's_R' refer to what sector the residual and input vectors represent. This can be seen by analyzing the original equation:

$$R_{nu} = +\Sigma_{i,a,\lambda}\, h_{ia}\langle u|\lambda\rangle C_{ain\lambda} \tag{28}$$

Where the residual has internal CAS character (as denoted by s_0) and the input vector **C** has 1h1p character. Proper configuration of these sectors means that the correct portions of each array are taken. In each case, only portions of a much larger array are used for each calculation. The offsets for each of the electrons that are part of this contribution are calculated based on what spin/representation is being looked at. Finally, the active space label is set by a subroutine that uses the previously calculated input sector. There are no active space electrons in this contribution, so this active space label does not change during this calculation.

```
do a = 1,na
     do i = 1,ni
          v2(a,i) = hmat(ioff+i,aoff+a)
```

Next, the local Hamiltonian array is filled in based on previously calculated particle numbers and offsets. This section allows the most flexibility in terms of how the calculation will proceed. Labels can be shuffled such the optimal matrix-matrix multiplication is achieved.

```
C_start = js_off_psi(s_C, arep, irep)
R_start = js_off_psi(s_R, 1, 1)
```

The offsets for both the **C** and **R** vectors are now calculated. Each offset is specific to the sector and representation currently being calculated. In this case, the residual vector only has one possible representation. This is a result of the residual sector being analyzed; the CAS space being the simplest possible space to calculate.

```
 nsum = na*ni
 nrow = 1
 ncol = nstate*nlambda
 fact = 1.0d0

 Call matrix-matrix multiplication
(nrow, ncol, nsum, fact,
 v2, maxorb,
 C(C_start), nsum,
 R(R_start), nrow)
```

A number of different values related to the matrix-matrix multiplication are first calculated. A matrix-matrix multiplication has the form shown in Equation 30, Where A and B are matrices, and M,K,N are the dimensions of each matrix. In the above, the internal label 'K' is represented by the variable 'nsum' and external labels M and N are represented by 'nrow' and 'ncol'. In effect, the internal labels disappear, and the external labels remain.

$$A[M \times K] \cdot B[K \times N] = C[M \times N] \tag{29}$$

In our previous psudeocode contribution:

$$R(1, n \cdot \lambda) = sum(i, a) \times V(1, i \cdot a) \cdot C(i \cdot a, n \cdot \lambda) \tag{30}$$

We are effectively summing over the inner labels in the Hamiltonian and Input vectors such that only the correct labels remain in the residual. The matrix-matrix multiplication used in BLAS will make sense of the calculation based on the supplied dimensions if the supplied dimensions results in a possible matrix multiplication.

The variable 'fact' is a factor that can apply to the result of the calculation, generally +/- 1. This sign is determined by how the different operators interact during the derivation of each contribution. Finally,

the matrix-matrix calculation is called with all the previously determined arguments. Essentially, the dimensions of the matrix and a resulting factor are given, as well as the matrices to be multiplied together. Finally, the matrix that this result is going to be placed in is also specified. In effect we have:

```
Call matrix-matrix multiplication
(Dimensions of the matrix (M,N,K)
(Matrix 1 with leading dimension)
(Matrix 2 with leading dimension)
(Result matrix with leading dimension)
```

To give the residual result. This call has many different arguments and is bulkier than many other matrix-matrix multiplication subroutines, but has incredible efficiency and flexibility. In each subroutine for each contribution, the matrix-matrix multiplication call will have roughly the same arguments but will be different depending on the contribution being calculated. This call is made extremely efficient by using the matrix-matrix multiplication function from the BLAS library.

4.2 Accounting for Spin Cases

The next subroutine that will be analyzed is a two-body contribution that has a number of different spin cases depending on the form of the two-electron integral, which all must be accounted for. This is accomplished by including an 'icase' parameter and careful manipulation of the contributing equations. In certain cases, these contributions end up being the same for all three cases. In some cases, this contribution can be entirely different for all three cases. This is determined by manipulating the equations for the two-electron integral based on the different allowed cases for spin, and the properties of two electron integrals. Any integrals that aren't entirely the same spin or that don't have equal amounts of alpha and beta spins are as shown in Equation 32. Dummy labels may be freely swapped if the character of the label is preserved. That is, hole labels can be swapped for hole labels, particle labels for particle labels, etc. as shown in Equation 33. With this in mind, operators may be permuted, and a sign is produced. After permuting these operators, labels can be swapped to 'line up' cases with other cases, if possible. Before checking for similar contributions, many different spin cases are considered in equation 34.

$$\langle AB|BB\rangle = \langle AA|AB\rangle = 0 \tag{31}$$

$$\langle XY|IJ\rangle = -\langle XY|JI\rangle \neq \langle XI|YJ\rangle \tag{32}$$

$$\langle AA|AA\rangle, \langle AB|AB\rangle, \langle AB|BA\rangle \tag{33}$$

The cases for the current contribution will now be examined. The equation for the all alpha case is shown in equation 35. This is the base example and requires no manipulation at this point. Next, the $\langle AB|AB\rangle$ spin case is examined in equation 36. Capital letters are used to denote electrons of different spin. This contribution is in the same form as the above, and requires no special manipulation. The different spins will simply have to be taken under consideration in the code. Lastly, the final $\langle AB|BA\rangle$ contribution is written as Equation 37.

$$R(d,l,n,\mu) = \langle dx|bl\rangle d^{\dagger}x^{\dagger}lb \cdot C(b,n,\lambda) \tag{34}$$

$$R(d,l,n,\mu) = \langle Dx|Bl\rangle D^{\dagger}x^{\dagger}lB \cdot C(B,n,\lambda) \tag{35}$$

$$R(d,l,n,\mu) = \langle Dx|bL\rangle D^{\dagger}x^{\dagger}Lb \cdot C(b,n,\lambda) \tag{36}$$

Which is not in the same form as the previous contribution. This contribution requires properties of the two body integrals to get it into the correct form. Namely that:

$$\langle AB|AB\rangle = -\langle AB|BA\rangle$$

This gives equation 38 which cannot be further modified. The 'L' and 'b' labels may not be swapped, as they refer to different categories of electrons; 'b' is a particle label and 'L' is a hole label.

$$R(d,l,n,\mu) = -\langle Dx|Lb\rangle D^{\dagger}x^{\dagger}Lb \cdot C(b,n,\lambda) \tag{37}$$

While in this contribution each case must be handled differently, other contributions can involve overlap between the cases. This can be shown by examining the 'F1' contribution. Equation 39 and 40 define the $\langle AB|AB\rangle$ term. Equation 39 is modified to Euqation 40 by permuting the 'Z' operator through 'y'.

F1: $R_{nu} = -\Sigma_{k,x,y,z,\lambda}\, \langle kx||zy\rangle\langle u|x^{\dagger}yz|\lambda\rangle C_{k\lambda}$ R(1,n;μ) = Sum(k) V(1,k) * C(k, n; λ)

$$R(n,\mu) = \langle Kx|Zy\rangle K^{\dagger}x^{\dagger}yZ \cdot C(k,n,\lambda) \tag{38}$$

$$R(n,\mu) = -\langle Kx|Zy\rangle K^{\dagger}x^{\dagger}Zy \cdot C(k,n,\lambda) \tag{39}$$

$$R(n,\mu) = \langle Kx|zY\rangle K^{\dagger}x^{\dagger}Yz \cdot C(k,n,\lambda) \tag{40}$$

Equation 41 shows the $\langle AB|BA\rangle$ term. This equation can be manipulated such that the two cases are the same, using operator permutations and label swaps. From Equation 42 to equation 43, the 'z' operator is permuted through 'Y', which introduces a factor of negative one. The next line is not technically necessary, but better shows that this case is equal to the previous case. This is because these labels have no further meaning besides representing an active electron. The label is summed over and is hence a 'dummy' label.

$$R(n,\mu) = \langle Kx|zY\rangle K^{\dagger}x^{\dagger}Yz \cdot C(k,n,\lambda) \tag{41}$$

$$R(n,\mu) = -\langle Kx|Yz\rangle K^{\dagger}x^{\dagger}Yz \cdot C(k,n,\lambda) \tag{42}$$

$$R(n,\mu) = -\langle Kx|Zy\rangle K^{\dagger}x^{\dagger}Zy \cdot C(k,n,\lambda) \tag{43}$$

4.3 Code Example of two body Hamiltonian

Once again, this example will start with the equation and pseudocode versions of the contribution which are shown in equation 45. This contribution is much more complicated than the one analyzed previously. Active space particles are involved which operate on the active space. This means that this label must be looped over explicitly, in addition to looping over the state label. Two body contributions must also all include all relevant spin cases, which means that each contribution must be run between one to three times depending on the complexity of the case. The code will be posted in its entirety, with sections of code analyzed. There are clear similarities to the previous contribution, which will not be gone over again in detail.

$$R_{ldnu} = -\Sigma_{x,b,d,l,\lambda}\, \langle dx||bl\rangle\langle u|x^{\dagger}|\lambda\rangle C_{b\lambda} \tag{44}$$

$$R(d\cdot l,n,\mu) = Sum(b)\, V(d\cdot l,b) \times c(b,n;\lambda)$$

```
do dspin=1,2
   do dx_rep=1, nirrep

      bl_rep = dx_rep
      do brep = 1, nirrep
         lrep = dirprd(brep, bl_rep)

         do drep=1, nirrep
            xrep=dirprd(drep, dx_rep)

            if (icase.eq.1) then
               bspin = dspin
               xspin = dspin
               lspin = dspin
               sfact = 1.0d0
            elseif (icase.eq.2) then
               bspin = dspin
               xspin = 3 - dspin
               lspin = 3 - dspin
               sfact = 1.0d0


          elseif (icase.eq.3) then
               lspin = dspin
               xspin = 3 - dspin
               bspin = 3 - dspin
               sfact = -1.0d0



               nb = js_norb(o_p, brep)
               nd = js_norb(o_p, drep)
               nl = js_norb(o_h, lrep)
               nx = js_norb(o_a, xrep)

               s_C = s_p(bspin)
               s_R = s_ph(dspin,lspin)

               doff = js_orb_offp(drep,dspin) -1
               loff = js_orb_offh(lrep,lspin) -1
               xoff = js_orb_offa(xrep,xspin) -1
               boff = js_orb_offp(brep,bspin) -1

               do x = 1,nx
                  do lambda = 1, js_nactive(s_C)
                     I_mu_1(x,lambda) = collect_I_mu_1
                                        (x,1,lambda, xrep,
                                         xspin, s_C, c_sign)
```

```
do x = 1,nx
   if (icase.eq.3) then
      do b = 1,nb
         do d = 1,nd
            do l = 1,nl
               v3(d,l,b) = hmat(doff+d,xoff+x,
                                loff+l,boff+b)
   else
      do b = 1,nb
         do d = 1,nd
            do l = 1,nl
               v3(d,l,b) = hmat(doff+d,xoff+x,
                                boff+b,loff+l)

   do lambda = 1,js_nactive(s_C)
      mu = I_mu_1(x,lambda)
      C_start = js_off_psi(s_C, brep, 1)
      R_start = js_off_psi(s_R, drep, lrep)

      nsum = nb
      nrow = nd*nl
      ncol = nstate
      nC = nb*nstate
      nR = nd * nl *  nstate
      fact = -1.0d0 * c_sign * sfact

      Call matrix-matrix multiplication
      (nrow, ncol, nsum, fact
       v3, maxorb,
       C(C_start + (lambda-1)*nC),nsum,
       R(R_start + (mu-1)*nR),nrow)
```

Next, we begin to discuss the different features of the two electron code beginning with a twist on the one electron code:

```
 do dspin=1,2
    do dx_rep=1, nirrep

       bl_rep = dx_rep
       do brep = 1, nirrep
          lrep = dirprd(brep, bl_rep)

          do drep=1, nirrep
             xrep=dirprd(drep, dx_rep)
```

Since each particles spin is relative to the other particles in the system, only one spin must be explicitly looped over. However, in the two-body case each representation is a product of the irreducible representations of the two related particles on each side of the integral. In this case, that means 'd'/'x' are related as well as 'b'/'l'. For the code, the result is that there is a product irreducible representation called 'dx_rep', which can be made by many different combinations of 'drep' and 'xrep'. 'drep' is looped over explicitly and a direct product function is used to find the related 'xrep'. Once the first irrep is found, the second irrep is found in a similar fashion. Of note is that the two product irreps are equal. This is a result of the symmetry of the two electron integrals.

```
if (icase.eq.1) then
   bspin = dspin
   xspin = dspin
   lspin = dspin
   sfact = 1.0d0
elseif (icase.eq.2) then
   bspin = dspin
   xspin = 3 - dspin
   lspin = 3 - dspin
   sfact = 1.0d0
elseif (icase.eq.3) then
   lspin = dspin
   xspin = 3 - dspin
   bspin = 3 - dspin
   sfact = -1.0d0
```

This is a simple if statement used to determine the spins of each particle based on which case is being looked at. Each case has an associated 'factor' related to how each case was derived. In this case, each spin case is different.

```
nb = js_norb(o_p, brep)
nd = js_norb(o_p, drep)
```

```
nl = js_norb(o_h, lrep)
nx = js_norb(o_a, xrep)

s_C = s_p(bspin)
s_R = s_ph(dspin,lspin)

doff = js_orb_offp(drep,dspin) -1
loff = js_orb_offh(lrep,lspin) -1
xoff = js_orb_offa(xrep,xspin) -1
boff = js_orb_offp(brep,bspin) -1
```

The above offsets and sectors are all calculated identically to the one body case. There are simply more of them to account for.

```
do x = 1,nx
     do lambda = 1, js_nactive(s_C)
          I_mu_1(x,lambda) = collect_I_mu_1(x,1,lambda, xrep,
                                            xspin, s_C, c_sign)
```

The above code is present in all contributions that include a change in the active space label. The purpose of this subroutine is to calculate each possible active space change based on each possible active particle and input active space configuration. These are placed into an array for later use during the matrix-matrix multiplication loops.

```
do x = 1,nx
     if (icase.eq.3) then
          do b = 1,nb
               do d = 1,nd
                    do l = 1,nl
                         v3(d,l,b) = hmat(doff+d,xoff+x,
                                     loff+l,boff+b)
     else
          do b = 1,nb
               do d = 1,nd
                    do l = 1,nl
                         v3(d,l,b) = hmat(doff+d,xoff+x,
                                     boff+b,loff+l)
```

Each Hamiltonian array is filled in based on the previous calculated offsets. Of note is that each case is functionally identical to the one body case with extra loops for extra particles, each Hamiltonian is filled in differently depending on the icase being analyzed.

```
do lambda = 1,js_nactive(s_C)
     mu = I_mu_1(x,lambda)
     C_start = js_off_psi(s_C, brep, 1)
     R_start = js_off_psi(s_R, drep, lrep)

     nsum = nb
     nrow = nd*nl
     ncol = nstate
     nC = nb*nstate
     nR = nd * nl * nstate
     fact = -1.0d0 * c_sign * sfact

     call B_GEMM('N','N',nrow,ncol,nsum,
                 fact,v3,js_maxorb,
                 C(C_start + (lambda-1)*nC),nsum,
                 1.0d0,
                 R(R_start + (mu-1)*nR),nrow)
```

Lastly, the matrix-matrix multiplication call is set up in a similar way to the previous contribution with one notable difference; each active state must be looped over explicitly. This time, the factor applied to each residual result is a product of the factor related to the spin case, the contribution in question, and the sign related to the calculation of 'mu'. This means that the offset calculated for both the residual and input vector is the offset for the first loop, with subsequent loops being shifted based by both 'nC' and 'nR'. Once again, these variables are filled in by examining the pseudocode representation of the contribution.

$$R(d \cdot l, n; \mu) = Sum(b)\, V(d \cdot l, b) \times c(b, n; \lambda) \tag{45}$$

In the previous calculation, this was accomplished implicitly. There was only one loop, and it included the entirety of the relevant parts of the C and R arrays. In this case, each lambda and mu is looped over

explicitly. The structure of each array means that looping over the more complicated sections last allows the program to loop as few times as possible.

4.4 Future Work Implementing the New Algorithm

As stated previously, the above CI code was not completed. While the code for each contribution was completed, subroutines within each contribution were not. These were included as 'black box' functions such that the code was able to compile, but do not function correctly. Even though the code could not be run, the compiler was used as a tool to check the code for bugs related to language semantics.

The most complicated 'black box' function that was not completed was the function responsible for taking input active spaces (λ) and converting them based on the active space operators present (x,y,z) to a new active space (μ). The idea behind this function would be to represent the input active space as a binary number with '1's representing an existing electron, then propagating every active space operator properly with a series of permutations while keeping track of the sign this produces. As a safety check, it should be possible for certain permutations to cause states to be annihilated resulting in the program gracefully exiting this failed contribution and continuing with another. Applying a creation operator to an existing electron or removing an electron that did not exist resulted in null states as shown in Equation 47 and 48. As per the rules of creation/annihilation operators. Equation 49 and 50 are also true for contributions that have multiple active space operators.

$$x^{\dagger}|a_0 \dots x_1 \dots\rangle = 0 \tag{46}$$

$$x|a_0 \dots x_0 \dots\rangle = 0 \tag{47}$$

$$x^{\dagger}x|a_0 \dots x_1 \dots\rangle = |a_0 \dots x_1 \dots\rangle \tag{48}$$

$$xx^{\dagger}|a_0 \dots x_0 \dots\rangle = |a_0 \dots x_0 \dots\rangle \tag{49}$$

$$xx^{\dagger}|a_0 \dots x_1 \dots\rangle = 0 \tag{50}$$

$$x^{\dagger}x|a_0 \dots x_0 \dots\rangle = 0 \tag{51}$$

The active space operators do not necessarily commute. The order of operators can also be swapped to produce two more properties. In both swapped cases the first operation annihilates the state. Equations 49 and 50 show operations that do not annihilate the state, while 51 and 52 do. Other unfinished sections of code include the calculation of the more complicated offset arrays, as well as a body of code responsible for running and accumulating each Hamiltonian contribution as well as performing all the necessary initial calculations related to the code.

In this chapter it has been shown that the matrix diagonalization step in the current implementation of MREOM takes by far the most time to complete, and is therefore the obvious target for the greatest gain in efficiency. By creating a data structure that takes advantage of incredibly optimized linear algebra subroutines, it is possible to compute multiple integrals in a single matrix-matrix multiplication call, whereas current implementations solve a single integral at a time. This is due to a one-size-fits-all solution in the current implementation, while the proposed code has a specialized subroutine for each individual contribution. This means that while coding the program becomes significantly more complicated, the time saved when calculating potential energy surfaces over multiple different systems is expected to be quite substantial. The algorithm is designed such that there is no resorting necessary to the CI vectors. The relevant elements of the Hamiltonian integrals are copied such that they can be efficiently entered into BLAS subroutines.

Chapter 5

Conclusion and Future Direction

MREOM-CC as a method has several desirable properties. The method can calculate many states from one set of amplitudes and a single state averaged CAS, and it is reasonably insensitive to the supplied CAS, which has less of an effect on the final results. As a method, MREOM has been previously used to calculate potential energy surfaces as well as vertical excitation spectra where single reference methods could not produce reasonable results. In this thesis, MREOM was examined using both a computational study designed to push the limits of the method and a new algorithm created to reduce the computational cost of the method. This new algorithm appears promising, but is unfinished currently. The computational study produced potential energy surfaces that were dubious in quality and does not appear to be a viable method for potential energy surface calculations.

It is often difficult to converge the full set of cluster amplitudes that enter the sequence of similarity transformations. To overcome this issue certain amplitudes are obtained from first-order perturbation theory. However, the selection of which amplitudes to treat using perturbation theory is ad hoc and can change with nuclear configuration. This is a prime reason potential energy surfaces can be discontinuous. Another reason may be the CI solver in the ORCA program, which may converge to different roots in unexpected ways. At present MR-EOMCC does not seem to be a viable approach to calculate full potential energy surfaces for a large number of states.

The MR-EOMCC approach does have its merits and in the future different avenues will be explored. One approach would be to construct vibronic models based on MREOM. Such calculations requires a sizable set of points at nearby geometries, such that numerical derivative approaches can be used to extract Taylor series expansion coefficients for the potential energy matrix in a diabatic representation. Since all displaced geometries are nearby, it should be straightforward to run consistent MREOM

calculations. Another schema would be to replace the CI amplitudes equations completely by a first-order perturbation theory. This would serve two purposes. First, one would expect continuous solutions as a function of nuclear geometry. Second, the approach would become substantially cheaper as the solution of cluster amplitudes is expensive. The choice of partitioning of $\widehat{H}$ into $H_o + V$ is crucial as a result, and this will need further investigation. If the cluster amplitudes are obtained by perturbation theory, the expense of MREOM is reduced.

In addition to the computational study, a new implementation of the MREOM-CC method was attempted to reduce the computational cost of MREOM calculations. This algorithm leveraged the efficiency of optimized BLAS subroutines by creating a new data type designed to exploit them. Indices are ordered in the data structure by complexity, with simpler labels like the particle and hole labels treated first and complex labels like the active space string being treated last. If indices appear in memory consecutively, then offsets can allow for the intelligent slicing of arrays such that contributions are calculated using the required pieces of arrays fed into a matrix-matrix BLAS multiplication subroutine. While this implementation is more efficient compared to the current implementation, it is much more complicated. Each contribution must be treated explicitly by a specifically tailored subroutine and aggregated. Currently, these contributions are treated with a general subroutine that sacrifices efficiency for simplicity.

In the future, the new algorithm will be implemented on ORCA in C++ as opposed to ACESII in FORTRAN. This means that the currently developed code will have to be ported, and the remaining body of code tying the contributions together will have to be written. As ORCA incorporates spin-orbit coupling where ACESII does not, this will result in a more useful calculation program. This new implementation will allow for the efficient testing of several different systems using the much faster code. Currently, using MREOM to calculate potential energy surfaces is unsatisfactory due to a few features introduced when calculating systems with complicated electronic structure. The new algorithm proposed in this thesis can

be used as a tool to open new calculation approaches hopefully allowing for more accurate calculations, either by using MREOM-CC as proposed in this study or by pairing it with a vibronic model. Nonetheless, further research and development is required.

References

1. C. D. Sherill, H. F. Schaefer; The Configuration Interaction Method: Advances in Highly Correlated. Advances in Quantum Chemistry 1999, 34, 143-269.

2. C. F. Fischer; General Hartree-Fock program. Computer Physics Communication 1987, 43 (3), 355-365.

3. H. G. Kummel; A Biography of the Coupled Cluster Method. International Journal of Modern Physics B 2003, 17 (28), 5311-5325.

4. D.I. Lyakh, M. Musial, V. F. Lotrich, R. J. Bartlett; Multireference Nature of Chemistry: The Coupled-Cluster View. Chemical Reviews 2012, 112 (1), 182-243.

5. H. J. Werner, P. J. Knowles; An efficient internally contracted multiconfiguration–reference configuration interaction method. Journal of Chemical Physics 1988, 89 (9), 5803.

6. D. Datta, M. Nooijen; Multireference Equation-of-Motion Coupled Cluster Theory. Journal of Chemical Physics 2012, 137 (20).

7. Z. Liu, L. M. J. Hunginton, M. Nooijen; Application of the multireference equation of motion coupled cluster method, including spin-orbit coupling, to the atomic spectra of Cr, Mn, Fe and Co. Molecular Physics 2015, 113 (19-20), 2999-3013.

8. Lee M. J. Huntington, M. Nooijen; Application of multireference equation of motion coupled-cluster theory to transition metal complexes and an orbital selection scheme for the efficient calculation of excitation energies. Journal of Chemical Physics 2015, 142 (19).

9. Lee M. J. Hunginton, O. Demel, M. Nooijen; Benchmark Applications of Variations of Multireference Equation of Motion Coupled-Cluster Theory. Journal Of Chemical Theory and Computation 2016, 12 (1), 114-132.

10. Eva Pavarini, Many-Electron States. https://www.cond-mat.de/events/correl13/manuscripts/koch.pdf (accessed Sept 27, 2017).

11. B. O. Roos, P. R. Taylor; A complete active space SCF method (CASSCF) using a density matrix formulated super-CI approach. Journal of Chemical Physics 1980, 48 (2), 157-173.

12. M. Nooijen; Computational Quantum Chemistry. http://scienide2.uwaterloo.ca/~nooijen/Chem-440-computational/MR_writeup.pdf (accessed Sept 27, 2017).

13. D. Mukherjee, W. Kutzelnigg; Normal order and extended Wick theorem for a multiconfiguration reference wave function. Journal of Chemical Physics 1997, 107 (2).

14. D. Datta, L. Kong, M. Nooijen; A state-specific partially internally contracted multireference coupled cluster approach. Journal of Chemical Physics 2011, 134 (21).

15. J. Yao ; The Electronic Structures of Cobalt-containing Diatomic Molecules. UWSpace 2016.

16. H. J. Werner, P. J. Knowles; An efficient internally contracted multiconfiguration–reference configuration interaction method. Journal of Chemical Physics 1988, 89 (9), 5803.

17. W. S. Hopkins; Chemistry 450 Course Notes; University of Waterloo, 2014.

18. Atomic Spectra Database Levels Form. https://physics.nist.gov/PhysRefData/ASD/levels_form.html (accessed Sept 28, 2017).

19. M. Nooijen; CHEM 400/740: Introduction to Computational Quantum Chemistry. http://scienide2.uwaterloo.ca/~nooijen/Chem-440-computational/CASSCF_and_NEVPT2_calculations.pdf (accessed 28 2017, 09).

20. F. Neese; ORCA Manual. https://cec.mpg.de/fileadmin/media/Forschung/ORCA/orca_manual_4_0_1.pdf (accessed Sept 28, 2017).

21. J. Zheng, X. Xu, D. G. Truhlar, Minimally augmented Karlsruhe basis sets. Theoretical Chemistry Accounts 2011, 128 (3), 295-305.

22. M. Reiher; Douglas–Kroll–Hess Theory: a relativistic electrons-only theory for chemistry. Theoretical Chemistry Accounts 2006, 116 (1-3), 241-252.

23. O. Demel, D. Datta, M. Nooijen; Additional global internal contraction in variations of multireference equation of motion coupled cluster theory. Journal of Chemical Physics 2013, 138 (13).

24. D. Datta, L. Kong, M. Nooijen; A state-specific partially internally contracted multireference coupled cluster approach. Journal of Chemical Physics 2011, 134 (21).

25. J. F. Harrison. Electronic Structure of Diatomic Molecules Composed of a First-Row Transition Metal and Main-Group Element (H−F). Chemical Reviews 2000 100 (2), 679-716

26. A. B. Anderson, R. W. Grimes, and S. Y. Hong; Toward a better understanding of the atom superposition and electron delocalization molecular orbital theory and a systematic test: diatomic oxides of the first transition-metal series, bonding and trends. The Journal of Physical Chemistry 1987 91 (16), 4245-4250

27. A. J. Merer; Spectroscopy of the Diatomic 3d Transition Metal Oxides. Annual Review of Physical Chemistry 1989 40:1, 407-438

28. A. Fiedler, D. Schroeder, S Shaik, H. Schwarz; Electronic Structures and Gas-Phase Reactivities of Cationic Late-Transition-Metal Oxides. Journal of the American Chemical Society 1994 116 (23), 10734-10741

29. Y. Nakao, K Hiaro; Theoretical study of first-row transition metal oxide cations. The Journal of Chemical Physics 114, 7935 (2001)

30. Y. Shiota, K. Yoshizawa; Methane-to-Methanol Conversion by First-Row Transition-Metal Oxide Ions: ScO^+, TiO^+,VO^+, CrO^+, MnO^+, FeO^+, CoO^+, NiO^+,and CuO^+. *Journal of the American Chemical Society* **2000** *122* (49), 12317-12326

31. J. Neugebauer, E. Baerends., M. Nooijen; Vibronic Structure of the Permanganate Absorption Spectrum from Time-Dependent Density Functional Calculations. Journal of Physical Chemistry 2005, 109 (6), 1168-1179.

Appendix A: List of Contributions to Hamiltonian in CI Code

The following list of contributions are grouped by the type of residual being evaluated, then by changing which input **C** vector was analyzed. Certain combinations were deemed impossible and then removed, but have been left in for completeness. The lettering alongside contributions was used to easily link subroutine filenames to a formula. Each subroutine's filename reflected the contribution it was calculating.

One Body Contributions

	~~$R_{nu} = \Sigma_{x,y,\lambda} h_{xy}\langle u\|x^{\ddagger}y\|\lambda\rangle C_{\lambda}$~~	
A.1	$R_{nu} = -\Sigma_{x,i,\lambda} h_{ix}\langle u\|x\|\lambda\rangle C_{in\lambda}$	R(1,n;mu) = -sum(i) V(1,i) * C(i,n; λ)
A.2	$R_{nu} = +\Sigma_{x,a,\lambda} h_{xa}\langle u\|x^{\dagger}\|\lambda\rangle C_{an\lambda}$	R(1,n;mu) = Sum(a) V(1,a) * C(a,n,;λ)
A.3	$R_{n\lambda} = +\Sigma_{i,a,\lambda} h_{ia}\langle u\|\lambda\rangle C_{ain\lambda}$	R(1,n*λ) = sum(i,a) V(1,i*a) * C(a*I,n*λ)
B.1	$R_{anu} = \Sigma_{x,a,\lambda} h_{ax}\langle u\|x\|\lambda\rangle C_{n\lambda}$	R(a,n;mu) = V(a,1) * C(1,n; λ)
B.2	$R_{anu} = +\Sigma_{a,b,\lambda} h_{ab}\langle u\|\lambda\rangle C_{bn\lambda}$	R(a,n* λ) = Sum(b) V(a,b) * C(b,n* λ)
	~~$R_{anu} = +\Sigma_{x,y,a,\lambda} h_{xy}\langle u\|x^{\ddagger}y\|\lambda\rangle C_{an\lambda}$~~	
B.3	$R_{anu} = -\Sigma_{x,a,i,\lambda} h_{ix}\langle u\|x\|\lambda\rangle C_{ain\lambda}$	R(a*n;mu) = sum(i) V(1,i) * C(a,i;n,λ)^T
C.1	$R_{inu} = -\Sigma_{x,i,\lambda} h_{xi}\langle u\|x^{\dagger}\|\lambda\rangle C_{n\lambda}$	R(i,n;mu) = V(i,1) * C(1,n;λ)
C.2	$R_{inu} = -\Sigma_{i,j,\lambda} h_{ij}\langle u\|\lambda\rangle C_{jn\lambda}$	R(i,n* λ) = V(i,j) * C(j,n* λ)
	~~$R_{inu} = +\Sigma_{x,y,j,\lambda} \delta_{ij} h_{xy}\langle u\|x^{\ddagger}y\|\lambda\rangle C_{in\lambda}$~~	
C.3	$R_{inu} = -\Sigma_{x,a,i,j,\lambda} h_{xa}\langle u\|x^{\dagger}\|\lambda\rangle C_{ain\lambda}$	R(i,n;mu) = V(1,a) * C(a,i,n;λ)
C.4	$R_{inu} = +\Sigma_{x,i,j,k,\lambda} h_{ix}\langle u\|x\|\lambda\rangle C_{ijn\lambda}$	R(i*n;mu) = sum(i) V(1,j) * C(i,j;n,λ)^T
D.1	$R_{ianu} = \Sigma_{a,i,\lambda} h_{ai}\langle u\|\lambda\rangle C_{n\lambda}$	R(i*a,n* λ) = V(i*a,1) * C(1,n* λ)
D.2	$R_{ianu} = -\Sigma_{x,i,j,a,\lambda} h_{ax}\langle u\|x\|\lambda\rangle C_{in\lambda}$	R(a,i*n; mu) = V(a,1) * C(1,i*n; λ)
D.3	$R_{ianu} = -\Sigma_{x,i,a,b,\lambda} \delta_{ab} h_{xi}\langle u\|x^{\dagger}\|\lambda\rangle C_{an\lambda}$	R(i,a*n;mu) = V(i,1) * C(1,a*n; λ)
D.4	$R_{ianu} = +\Sigma_{i,j,a,b,\lambda} h_{ba}\langle u\|\lambda\rangle C_{bin\lambda}$	R(a,i*n* λ) = sum(b) V(a,b) * C(b,i*n* λ)
D.5	$R_{ianu} = -\Sigma_{a,b,ij,\lambda} h_{ij}\langle u\|\lambda\rangle C_{ajn\lambda}$	R(i,a*n* λ) = sum(j) V(i,j) * C(a,j;n,λ)^T
~~$R_{ianu} = +\Sigma_{x,y,a,b,i,j,\lambda} h_{xy}\delta_{ab}\delta_{ij}\langle u\|x^{\ddagger}y\|\lambda\rangle C_{bjn\lambda}$~~		
E.1	$R_{ijn\lambda} = \Sigma_{i,j,n,\lambda} h_{xj}\langle u\|x^{\dagger}\|\lambda\rangle C_{i,n,\lambda}$	R(j,i*n;mu) = V(j,1) *C(1,i*n;λ)
~~$R_{i,j,n,\lambda} = \Sigma_{i,j,k,l,n,\lambda} \delta_{jk}\delta_{il} h_{xy}\langle u\|x^{\ddagger}y\|\lambda\rangle C_{k,l,n,\lambda}$~~		
E.2	$R_{ijn\lambda} = \Sigma_{i,j,k,l,n,\lambda} h_{kj}\langle u\|\lambda\rangle C_{k,i,n,\lambda}$	R(j,i*n* λ) = sum(k) V(j,k) * C(k,i*n*λ)

Two Body Contributions

	~~$\langle u\|\{p^\ddagger q^\ddagger rs\}\|\lambda\rangle$~~	~~$R_{nu} = \Sigma_{w,x,y,z,\lambda} \langle xy\|\|wz\rangle\langle u\|x^\ddagger y^\ddagger zw\|\lambda\rangle C_\lambda$~~
F.1	$\langle u\|\{p^\dagger q^\dagger rs\}k\|\lambda\rangle$	$R_{nu} = -\Sigma_{k,x,y,z,\lambda} \langle kx\|\|zy\rangle\langle u\|x^\dagger yz\|\lambda\rangle C_{k\lambda}$
F.2	$\langle u\|\{p^\dagger q^\dagger rs\}b^\dagger\|\lambda\rangle$	$R_{nu} = +\Sigma_{b,x,y,z,\lambda} \langle xy\|\|bz\rangle\langle u\|x^\dagger y^\dagger z\|\lambda\rangle C_{b\lambda}$
F.3	$\langle u\|\{p^\dagger q^\dagger rs\}b^\dagger k\|\lambda\rangle$	$R_{nu} = -\Sigma_{x,y,k,b,\lambda} \langle xk\|\|by\rangle\langle u\|x^\dagger y\|\lambda\rangle C_{bk\lambda}$
F.4	$\langle u\|\{p^\dagger q^\dagger rs\}jk\|\lambda\rangle$	$R_{nu} = +\Sigma_{x,y,j,k,\lambda} \langle jk\|\|yx\rangle\langle u\|xy\|\lambda\rangle C_{jk\lambda}$
G.1	$\langle u\|d\{p^\dagger q^\dagger rs\}\|\lambda\rangle$	$R_{ndu} = \Sigma_{x,y,z,d,\lambda} \langle dx\|\|zy\rangle\langle u\|x^\dagger yz\|\lambda\rangle C_\lambda$
G.2	$\langle u\|d\{p^\dagger q^\dagger rs\}k\|\lambda\rangle$	$R_{ndu} + \Sigma_{x,y,k,d,\lambda} \langle dk\|\|yx\rangle\langle u\|xy\|\lambda\rangle C_{k\lambda}$
	~~$\langle u\|d\{p^\ddagger q^\ddagger rs\}b^\ddagger\|\lambda\rangle$~~	~~$R_{ndu} + \Sigma_{w,x,y,z,d,b,\lambda} \delta_{db}\langle xy\|\|wz\rangle\langle u\|x^\ddagger y^\ddagger wz\|\lambda\rangle C_{b\lambda}$~~
G.3	$\langle u\|d\{p^\dagger q^\dagger rs\}b^\dagger\|\lambda\rangle$	$R_{ndu} + \Sigma_{x,y,b,d,\lambda} \langle dx\|\|by\rangle\langle u\|x^\dagger y\|\lambda\rangle C_{b\lambda}$
G.4	$\langle u\|d\{p^\dagger q^\dagger rs\}b^\dagger k\|\lambda\rangle$	$R_{ndu} + \Sigma_{x,y,z,k,b,d,\lambda} \delta_{db}\langle xk\|\|zy\rangle\langle u\|x^\dagger yz\|\lambda\rangle C_{bk\lambda}$
G.5	$\langle u\|d\{p^\dagger q^\dagger rs\}b^\dagger k\|\lambda\rangle$	$R_{ndu} - \Sigma_{x,k,b,d,\lambda} \langle dk\|\|bx\rangle\langle u\|x\|\lambda\rangle C_{bk\lambda}$
	~~$\langle u\|d\{p^\ddagger q^\ddagger rs\}jk\|\lambda\rangle$~~	
H.1	$\langle u\|l^\dagger\{p^\dagger q^\dagger rs\}\|\lambda\rangle$	$R_{nlu} = \Sigma_{x,y,z,l,\lambda} \langle xy\|\|zl\rangle\langle u\|x^\dagger y^\dagger z\|\lambda\rangle C_\lambda$
	~~$\langle u\|l^\ddagger\{p^\ddagger q^\ddagger rs\}k\|\lambda\rangle$~~	~~$R_{nlu} = +\Sigma_{w,x,y,z,l,k,\lambda} \delta_{lk}\langle xy\|\|wz\rangle\langle u\|x^\ddagger y^\ddagger zw\|\lambda\rangle C_{k\lambda}$~~
H.2	$\langle u\|l^\dagger\{p^\dagger q^\dagger rs\}k\|\lambda\rangle$	$R_{nlu} = -\Sigma_{x,y,k,l,\lambda} \langle xk\|\|yl\rangle\langle u\|x^\dagger y\|\lambda\rangle C_{k\lambda}$
H.3	$\langle u\|l^\dagger\{p^\dagger q^\dagger rs\}b^\dagger\|\lambda\rangle$	$R_{nlu} = +\Sigma_{x,y,b,l,\lambda} \langle xy\|\|bl\rangle\langle u\|x^\dagger y^\dagger\|\lambda\rangle C_{b\lambda}$
H.4	$\langle u\|l^\dagger\{p^\dagger q^\dagger rs\}b^\dagger k\|\lambda\rangle$	$R_{nlu} = -\Sigma_{x,y,z,b,l,k\lambda} \delta_{lk}\langle xy\|\|bz\rangle\langle u\|x^\dagger y^\dagger z\|\lambda\rangle C_{bk\lambda}$
H.5	$\langle u\|l^\dagger\{p^\dagger q^\dagger rs\}b^\dagger k\|\lambda\rangle$	$R_{nlu} = +\Sigma_{x,k,l,b,\lambda} \langle xk\|\|bl\rangle\langle u\|x^\dagger\|\lambda\rangle C_{bk\lambda}$
H.6	$\langle u\|l^\dagger\{p^\dagger q^\dagger rs\}jk\|\lambda\rangle$	$R_{nlu} = -\Sigma_{x,k,l,b,\lambda} \delta_{lk}\langle xj\|\|zy\rangle\langle u\|x^\dagger yz\|\lambda\rangle C_{jk\lambda}$
I.1	$\langle u\|l^\dagger d\{p^\dagger q^\dagger rs\}\|\lambda\rangle$	$R_{nldu} = -\Sigma_{x,y,d,l,\lambda} \langle dx\|\|yl\rangle\langle u\|x^\dagger y\|\lambda\rangle C_\lambda$
I.2	$\langle u\|l^\dagger d\{p^\dagger q^\dagger rs\}b^\dagger\|\lambda\rangle$	$R_{nldu} = +\Sigma_{x,y,z,b,d,l,\lambda} \delta_{db}\langle xy\|\|zl\rangle\langle u\|x^\dagger y^\dagger z\|\lambda\rangle C_{b\lambda}$
I.3	$\langle u\|l^\dagger d\{p^\dagger q^\dagger rs\}b^\dagger\|\lambda\rangle$	$R_{nldu} = -\Sigma_{x,b,d,l,\lambda} \langle dx\|\|bl\rangle\langle u\|x^\dagger\|\lambda\rangle C_{b\lambda}$
I.4	$\langle u\|l^\dagger d\{p^\dagger q^\dagger rs\}k\|\lambda\rangle$	$R_{nldu} = -\Sigma_{x,y,z,d,l,k,\lambda} \delta_{lk}\langle dx\|\|zy\rangle\langle u\|x^\dagger y^\dagger\|\lambda\rangle C_{k\lambda}$
I.5	$\langle u\|l^\dagger d\{p^\dagger q^\dagger rs\}k\|\lambda\rangle$	$R_{nldu} = +\Sigma_{x,d,l,k,\lambda} \langle dk\|\|xl\rangle\langle u\|x\|\lambda\rangle C_{k\lambda}$
	~~$\langle u\|l^\ddagger d\{p^\ddagger q^\ddagger rs\}b^\ddagger k\|\lambda\rangle$~~	~~$R_{nldu} = +\Sigma_{w,x,y,z,b,d,l,k,\lambda} \delta_{lk}\delta_{db}\langle xy\|\|wz\rangle\langle u\|x^\ddagger y^\ddagger zw\|\lambda\rangle C_{bk\lambda}$~~
I.6	$\langle u\|l^\dagger d\{p^\dagger q^\dagger rs\}b^\dagger k\|\lambda\rangle$	$R_{nldu} = -\Sigma_{b,d,l,k,\lambda} \langle dk\|\|bl\rangle\langle u\|\lambda\rangle C_{bk\lambda}$
I.7	$\langle u\|l^\dagger d\{p^\dagger q^\dagger rs\}b^\dagger k\|\lambda\rangle$	$R_{nldu} = +\Sigma_{x,y,b,l,k,\lambda} \delta_{lk}\langle dx\|\|by\rangle\langle u\|x^\dagger y\|\lambda\rangle C_{bk\lambda}$
I.8	$\langle u\|l^\dagger d\{p^\dagger q^\dagger rs\}b^\dagger k\|\lambda\rangle$	$R_{nldu} = -\Sigma_{x,y,z,b,d,l,\lambda} \delta_{db}\langle xk\|\|yl\rangle\langle u\|x^\dagger y\|\lambda\rangle C_{bk\lambda}$
I.9	$\langle u\|l^\dagger d\{p^\dagger q^\dagger rs\}jk\|\lambda\rangle$	$R_{nldu} = +\Sigma_{x,y,j,k,\lambda} \delta_{lk}\langle dj\|xy\rangle\langle u\|xy\|\lambda\rangle C_{jk\lambda}$

J.1	$\langle u\|m^\dagger n^\dagger\{p^\dagger q^\dagger rs\}\|\lambda\rangle$	$R_{mnu} = \Sigma_{x,y,m,n,\lambda}\,\langle xy\|\|mn\rangle\langle u\|x^\dagger y^\dagger\|\lambda\rangle C_\lambda$
J.2	$\langle u\|m^\dagger n^\dagger\{p^\dagger q^\dagger rs\}k\|\lambda\rangle$	$R_{mnu} = +\Sigma_{x,k,m,n,\lambda}\,\langle xk\|\|mn\rangle\langle u\|x^\dagger\|\lambda\rangle C_{k\lambda}$
J.3	$\langle u\|m^\dagger n^\dagger\{p^\dagger q^\dagger rs\}k\|\lambda\rangle$	$R_{mnu} = -\Sigma_{x,y,z,n,m,k,\lambda}\,\delta_{nk}\langle xy\|\|mz\rangle\langle u\|x^\dagger y^\dagger z\|\lambda\rangle C_{k\lambda}$
J.4	$\langle u\|m^\dagger n^\dagger\{p^\dagger q^\dagger rs\}b^\dagger\|\lambda\rangle$	$R_{mnu} = +\Sigma_{x,y,b,n,m,k,\lambda}\,\delta_{mk}\langle xy\|\|bn\rangle\langle u\|x^\dagger y^\dagger\|\lambda\rangle C_{bk\lambda}$
	~~$\langle u\|m^\dagger n^\dagger\{p^\dagger q^\dagger rs\}b^\dagger k\|\lambda\rangle$~~	
J.5	$\langle u\|m^\dagger n^\dagger\{p^\dagger q^\dagger rs\}jk\|\lambda\rangle$	$R_{mnu} = -\Sigma_{x,y,j,k,m,n,\lambda}\,\delta_{nj}\langle xk\|\|ym\rangle\langle u\|x^\dagger y\|\lambda\rangle C_{jk\lambda}$
J.6	$\langle u\|m^\dagger n^\dagger\{p^\dagger q^\dagger rs\}jk\|\lambda\rangle$	$R_{mnu} = +\Sigma_{w,x,y,z,j,k,m,n,\lambda}\delta_{nj}\delta_{mk}\langle xy\|\|wz\rangle\langle u\|x^\dagger y^\dagger zw\|\lambda\rangle C_{jk\lambda}$
J.7	$\langle u\|m^\dagger n^\dagger\{p^\dagger q^\dagger rs\}jk\|\lambda\rangle$	$R_{mnu} = +\Sigma_{k,j,m,n,\lambda}\,\langle kj\|\|mn\rangle\langle u\|\lambda\rangle C_{jk\lambda}$

Appendix B: Complete Active Space Orbital Occupancies

The following are orbital occupancy tables related to CASSCF calculations of the molecules studied in Chapter 2. The values listed are the expected value of electrons found in that orbital.

High Spin CAS Orbital Occupancies

VO^+

Distance (A)	Orbital occupancys								
1.45	1	1	1	1	0.8	0.8	0.8	0.8	0.8
1.5	1	1	1	1	0.8	0.8	0.8	0.8	0.8
1.55	1	1	1	1	0.8	0.8	0.8	0.8	0.8
1.6	1	1	1	1	0.8	0.8	0.8	0.8	0.8
1.65	1	1	1	1	0.8	0.8	0.8	0.8	0.8
1.7	1	1	1	1	0.8	0.8	0.8	0.8	0.8
1.75	1	1	1	1	0.8	0.8	0.8	0.8	0.8
1.8	1	1	1	1	0.8	0.8	0.8	0.8	0.8
1.85	1	1	1	1	0.8	0.8	0.8	0.8	0.8
1.9	1	1	1	1	0.8	0.8	0.8	0.8	0.8
1.95	1	1	1	1	0.8	0.8	0.8	0.8	0.8
2.0	1	1	1	1	0.8	0.8	0.8	0.8	0.8
2.05	1	1	1	1	0.8	0.8	0.8	0.8	0.8
2.1	1	1	1	1	0.8	0.8	0.8	0.8	0.8
2.2	1	1	1	1	0.8	0.8	0.8	0.8	0.8
2.3	1	1	1	1	0.8	0.8	0.8	0.8	0.8

CrO^+

Distance (Å)	Orbital occupancys								
1.4	0.25	0.25	0.25	0.25	0.25	0.25	0.25	0.25	0.25
1.45	0.25	0.25	0.25	0.25	0.25	0.25	0.25	0.25	0.25
1.5	0.25	0.25	0.25	0.25	0.25	0.25	0.25	0.25	0.25
1.55	0.25	0.25	0.25	0.25	0.25	0.25	0.25	0.25	0.25
1.6	0.25	0.25	0.25	0.25	0.25	0.25	0.25	0.25	0.25
1.65	0.25	0.25	0.25	0.25	0.25	0.25	0.25	0.25	0.25
1.7	0.25	0.25	0.25	0.25	0.25	0.25	0.25	0.25	0.25
1.75	0.25	0.25	0.25	0.25	0.25	0.25	0.25	0.25	0.25
1.8	0.25	0.25	0.25	0.25	0.25	0.25	0.25	0.25	0.25
1.85	0.25	0.25	0.25	0.25	0.25	0.25	0.25	0.25	0.25
1.9	0.25	0.25	0.25	0.25	0.25	0.25	0.25	0.25	0.25
1.95	0.25	0.25	0.25	0.25	0.25	0.25	0.25	0.25	0.25
2.0	0.25	0.25	0.25	0.25	0.25	0.25	0.25	0.25	0.25
2.05	0.25	0.25	0.25	0.25	0.25	0.25	0.25	0.25	0.25
2.1	0.25	0.25	0.25	0.25	0.25	0.25	0.25	0.25	0.25
2.2	0.25	0.25	0.25	0.25	0.25	0.25	0.25	0.25	0.25

MnO^+

Distance (Å)	Orbital occupancys								
1.4	1.2	1.2	1.2	1.2	1.2	1	1	1	1
1.45	1.2	1.2	1.2	1.2	1.2	1	1	1	1
1.5	1.2	1.2	1.2	1.2	1.2	1	1	1	1
1.55	1.2	1.2	1.2	1.2	1.2	1	1	1	1
1.6	1.2	1.2	1.2	1.2	1.2	1	1	1	1
1.65	1.2	1.2	1.2	1.2	1.2	1	1	1	1
1.7	1.2	1.2	1.2	1.2	1.2	1	1	1	1
1.75	1.2	1.2	1.2	1.2	1.2	1	1	1	1
1.8	1.2	1.2	1.2	1.2	1.2	1	1	1	1
1.85	1.2	1.2	1.2	1.2	1.2	1	1	1	1
1.9	1.2	1.2	1.2	1.2	1.2	1	1	1	1
1.95	1.2	1.2	1.2	1.2	1.2	1	1	1	1
2.0	1.2	1.2	1.2	1.2	1.2	1	1	1	1
2.2	1.2	1.2	1.2	1.2	1.2	1	1	1	1

FeO^+

Distance (Å)	Orbital occupancys								
1.4	1.5625	1.5625	1.3908	1.384	1.0375	1.0375	1.016	1.0091	1
1.45	1.7481	1.3785	1.3785	1.1997	1.1997	1.0509	1.0224	1.0224	1
1.5	1.7437	1.3723	1.3723	1.1997	1.1997	1.0553	1.0284	1.0284	1
1.55	1.7393	1.3643	1.3643	1.1998	1.1998	1.0597	1.0363	1.0363	1
1.6	1.7362	1.3548	1.3548	1.1999	1.1999	1.0629	1.0458	1.0458	1
1.65	1.7358	1.3446	1.3446	1.2	1.2	1.0633	1.0559	1.0559	1
1.7	1.7387	1.3347	1.3347	1.2	1.2	1.0657	1.0657	1.0604	1
1.75	1.7446	1.3261	1.3261	1.2001	1.2001	1.0743	1.0743	1.0545	1
1.8	1.7525	1.3192	1.3192	1.2001	1.2001	1.0811	1.0811	1.0466	1
1.85	1.761	1.3141	1.3141	1.2001	1.2001	1.0862	1.0862	1.0382	1
1.9	1.9714	1.2255	1.2001	1.2001	1.1871	1.1871	1.0136	1.0136	1.0014
1.95	1.9778	1.2197	1.2001	1.2001	1.1899	1.1899	1.0107	1.0107	1.0011
2.0	1.9829	1.2151	1.2001	1.2001	1.1921	1.1921	1.0083	1.0083	1.0009
2.05	1.9868	1.2115	1.2001	1.2001	1.194	1.194	1.0065	1.0065	1.0007
2.1	1.9898	1.2088	1.2001	1.2001	1.1954	1.1954	1.005	1.005	1.0005
2.15	1.9921	1.2067	1.2001	1.2001	1.1964	1.1964	1.0039	1.0039	1.0004
2.2	1.9939	1.2051	1.2001	1.2001	1.1972	1.1972	1.003	1.003	1.0003

CoO^+

Distance (Å)	Orbital occupancys								
1.3	1.7626	1.7626	1.5815	1.398	1.398	1.0371	1.0371	1.0231	1
1.35	1.9662	1.5643	1.5643	1.3997	1.3997	1.0354	1.0354	1.0351	1.0001
1.4	1.9619	1.5602	1.5602	1.3995	1.3995	1.0401	1.0392	1.0392	1.0002
1.45	1.9539	1.5549	1.5549	1.3992	1.3992	1.0492	1.0442	1.0442	1.0002
1.5	1.9351	1.5459	1.5459	1.3987	1.3987	1.0707	1.0524	1.0524	1.0003
1.55	1.9053	1.5329	1.5329	1.3976	1.3976	1.1064	1.0634	1.0634	1.0005
1.6	1.8831	1.5232	1.5232	1.3959	1.3959	1.1384	1.0697	1.0697	1.0007
1.65	1.8791	1.5211	1.5211	1.3936	1.3936	1.1559	1.0673	1.0673	1.0009
1.7	1.8924	1.5256	1.5256	1.391	1.391	1.1583	1.0575	1.0575	1.0011
1.75	1.9141	1.533	1.533	1.3884	1.3884	1.1522	1.0448	1.0448	1.0011
1.8	1.9355	1.54	1.54	1.3861	1.3861	1.1447	1.0332	1.0332	1.0011
1.85	1.9529	1.5454	1.5454	1.3841	1.3841	1.1389	1.0241	1.0241	1.001
1.9	1.9659	1.5493	1.5493	1.3824	1.3824	1.1353	1.0173	1.0173	1.0008
1.95	1.9752	1.552	1.552	1.3807	1.3807	1.1337	1.0125	1.0125	1.0007
2.0	1.9819	1.5538	1.5538	1.3791	1.3791	1.1333	1.0091	1.0091	1.0006
2.2	1.9945	1.5575	1.5575	1.3734	1.3734	1.1379	1.0027	1.0027	1.0002

NiO^+

Distance (Å)	Orbital occupancys								
1.45	1.9064	1.6968	1.6968	1.6909	1.6909	1.1155	1.1011	1.1011	1.0006
1.5	1.8835	1.6984	1.6984	1.6816	1.6816	1.1555	1.1001	1.1001	1.0008
1.55	1.8682	1.6941	1.6941	1.6786	1.6786	1.1969	1.0942	1.0942	1.001
1.65	1.8859	1.6945	1.6945	1.6729	1.6729	1.2477	1.0651	1.0651	1.0013
1.7	1.9095	1.7069	1.7069	1.6615	1.6615	1.2545	1.049	1.049	1.0012
1.75	1.9318	1.7178	1.7178	1.6518	1.6518	1.2561	1.0359	1.0359	1.0011
1.85	1.9635	1.7328	1.7328	1.6379	1.6379	1.257	1.0187	1.0187	1.0008
1.9	1.9734	1.7374	1.7374	1.6329	1.6329	1.2582	1.0136	1.0136	1.0006
1.95	1.9805	1.7408	1.7408	1.6287	1.6287	1.2601	1.0099	1.0099	1.0005
2.05	1.9894	1.745	1.745	1.6223	1.6223	1.2649	1.0054	1.0054	1.0003
2.1	1.9921	1.7463	1.7463	1.6198	1.6198	1.2675	1.004	1.004	1.0003
2.2	1.9955	1.7479	1.7479	1.6157	1.6157	1.2725	1.0022	1.0022	1.0002

Low Spin CAS Orbital Occupancies

VO^+

Distance (Å)	Orbital occupancys						
1.45	1.9828	1.008	0.9564	0.9542	0.4064	0.3509	0.3412
1.5	1.9721	1.0197	0.949	0.9471	0.4105	0.3518	0.3498
1.55	1.498	1.498	0.943	0.943	0.502	0.502	0.1141
1.6	1.4982	1.4982	0.9329	0.9329	0.5018	0.5018	0.1342
1.65	1.4983	1.4983	0.9224	0.9224	0.5016	0.5016	0.1552
1.7	1.4985	1.4985	0.9115	0.9115	0.5015	0.5015	0.177
1.75	1.4987	1.4987	0.9005	0.9005	0.5013	0.5013	0.1992
1.8	1.4988	1.4988	0.8893	0.8893	0.5011	0.5011	0.2214
1.85	1.499	1.499	0.8783	0.8783	0.501	0.501	0.2434
1.9	1.4991	1.4991	0.8676	0.8676	0.5009	0.5009	0.2649
1.95	1.4992	1.4992	0.8572	0.8572	0.5007	0.5007	0.2856
2.0	1.4993	1.4993	0.8473	0.8473	0.5006	0.5006	0.3054
2.05	1.206	1.206	0.7939	0.7939	0.6668	0.6668	0.6666
2.1	1.1783	1.1783	0.8216	0.8216	0.6667	0.6667	0.6666

CrO^+

Distance (Å)	Orbital occupancys								
1.4	1.7826	1.7826	1.3368	0.9981	0.9981	0.9734	0.5496	0.5496	0.0292
1.45	1.9437	1.4931	1.493	0.9972	0.9972	0.8401	0.8401	0.3703	0.0251
1.5	1.951	1.4896	1.4896	0.9976	0.9976	0.8435	0.8435	0.3631	0.0244
1.55	1.954	1.4881	1.4881	0.998	0.998	0.845	0.845	0.3599	0.0239
1.65	1.9563	1.4871	1.4871	0.9985	0.9985	0.846	0.846	0.357	0.0235
1.7	1.9562	1.4871	1.4871	0.9987	0.9987	0.846	0.846	0.3563	0.0239
1.75	1.9552	1.487	1.487	0.9989	0.9989	0.8461	0.8461	0.356	0.0249
1.85	1.9502	1.4864	1.4864	0.9991	0.9991	0.8467	0.8467	0.3565	0.0289
1.9	1.9458	1.4857	1.4857	0.9992	0.9992	0.8474	0.8473	0.3576	0.0321
1.95	1.9397	1.4847	1.4846	0.9993	0.9993	0.8484	0.8484	0.3595	0.0361
2.0	1.9311	1.483	1.4829	0.9994	0.9994	0.8501	0.8501	0.3626	0.0414
2.05	1.9193	1.4803	1.4803	0.9994	0.9994	0.8527	0.8527	0.3677	0.0481
2.1	1.6913	1.418	1.418	0.9996	0.9996	0.9149	0.9149	0.6002	0.0436

MnO^+

Distance (Å)	Orbital occupancys							
1.4	1.9145	1.8954	1.8954	1.0008	1.0008	0.7713	0.7713	0.7505
1.45	1.8975	1.8724	1.8724	1.0007	1.0007	0.7943	0.7943	0.7677
1.5	1.8792	1.8462	1.8462	1.0006	1.0006	0.8204	0.8204	0.7864
1.55	1.8594	1.8182	1.8182	1.0004	1.0004	0.8484	0.8484	0.8066
1.6	1.8384	1.7904	1.7904	1.0003	1.0003	0.8761	0.8761	0.828
1.65	1.8169	1.765	1.765	1.0002	1.0002	0.9014	0.9014	0.8499
1.7	1.7958	1.7435	1.7435	1.0001	1.0001	0.9229	0.9229	0.8713
1.75	1.776	1.7262	1.7262	1	1	0.9402	0.9402	0.8912
1.8	1.7581	1.7128	1.7128	1	1	0.9536	0.9536	0.9091
1.85	1.7427	1.7027	1.7027	1	1	0.9637	0.9637	0.9245
1.9	1.7298	1.695	1.695	0.9999	0.9999	0.9714	0.9714	0.9374
1.95	1.7191	1.6892	1.6892	0.9999	0.9999	0.9773	0.9773	0.948
2.0	1.7104	1.6848	1.6848	1	1	0.9817	0.9817	0.9567

FeO^+

Distance (Å)	Orbital occupancys								
1.45	1.748	1.3784	1.3784	1.1997	1.1997	1.0509	1.0225	1.0225	1
1.5	1.7436	1.3723	1.3723	1.1997	1.1997	1.0554	1.0285	1.0285	1
1.55	1.7393	1.3643	1.3643	1.1998	1.1998	1.0598	1.0364	1.0364	1
1.6	1.7362	1.3547	1.3547	1.1999	1.1999	1.0629	1.0458	1.0458	1
1.65	1.7357	1.3445	1.3445	1.2	1.2	1.0633	1.056	1.056	1
1.7	1.7387	1.3347	1.3347	1.2	1.2	1.0657	1.0657	1.0604	1
1.75	1.7446	1.3261	1.3261	1.2001	1.2001	1.0743	1.0743	1.0545	1
1.8	1.7526	1.3192	1.3192	1.2001	1.2001	1.0811	1.0811	1.0466	1
1.85	1.761	1.3141	1.3141	1.2001	1.2001	1.0862	1.0862	1.0381	1
1.9	1.9713	1.2256	1.2001	1.2001	1.1871	1.1871	1.0136	1.0136	1.0014
1.95	1.9778	1.2197	1.2001	1.2001	1.1899	1.1899	1.0107	1.0107	1.0011
2.0	1.9828	1.2151	1.2001	1.2001	1.1921	1.1921	1.0084	1.0084	1.0009
2.05	1.9868	1.2115	1.2001	1.2001	1.1939	1.1939	1.0065	1.0065	1.0007
2.1	1.9898	1.2088	1.2001	1.2001	1.1953	1.1953	1.005	1.005	1.0005
2.15	1.9921	1.2067	1.2001	1.2001	1.1964	1.1964	1.0039	1.0039	1.0004
2.2	1.9938	1.2052	1.2001	1.2001	1.1972	1.1972	1.0031	1.0031	1.0003

CoO^+

Distance (Å)	Orbital occupancys								
1.3	1.9532	1.9532	1.9235	1.4992	1.4992	1.0463	1.0463	1.0257	0.0532
1.35	1.9439	1.9439	1.9183	1.4989	1.4989	1.0557	1.0557	1.0339	0.0508
1.4	1.9328	1.9328	1.9139	1.4986	1.4986	1.0668	1.0668	1.0421	0.0478
1.45	1.9199	1.9199	1.9106	1.498	1.498	1.0797	1.0797	1.0494	0.0447
1.5	1.9094	1.9051	1.9051	1.4972	1.4972	1.0945	1.0945	1.055	0.0419
1.55	1.9111	1.888	1.888	1.4961	1.4961	1.1116	1.1116	1.0581	0.0394
1.6	1.9162	1.8685	1.8685	1.4947	1.4947	1.1311	1.1311	1.0582	0.0371
1.65	1.9238	1.8468	1.8468	1.4929	1.4929	1.1528	1.1528	1.0558	0.0354
1.7	1.9312	1.824	1.824	1.4909	1.4909	1.1756	1.1756	1.0521	0.0355
1.75	1.9367	1.801	1.801	1.4889	1.4889	1.1987	1.1987	1.0486	0.0376
1.8	1.9393	1.778	1.778	1.487	1.4869	1.2216	1.2216	1.0461	0.0414
1.85	1.9384	1.7554	1.7554	1.4853	1.485	1.2442	1.2442	1.0449	0.0472
1.9	1.9339	1.7333	1.7333	1.4836	1.4834	1.2664	1.2664	1.0445	0.0555
1.95	1.9249	1.7113	1.7113	1.4824	1.4819	1.2883	1.2883	1.0443	0.0673
2.0	1.9103	1.6893	1.6893	1.4812	1.4808	1.3103	1.3103	1.044	0.0846

NiO^+

Distance (Å)	Orbital occupancys								
1.4	1.9434	1.91	1.91	1.6693	1.6693	1.6565	1.0913	1.0913	0.0588
1.45	1.942	1.8962	1.8962	1.6708	1.6708	1.6561	1.1051	1.1051	0.0577
1.5	1.9411	1.8802	1.8802	1.6725	1.6725	1.6545	1.1209	1.1209	0.0571
1.55	1.9409	1.8614	1.8614	1.6742	1.6742	1.652	1.1396	1.1396	0.0568
1.6	1.9414	1.8389	1.8389	1.6756	1.6756	1.6493	1.1619	1.1619	0.0566
1.65	1.9422	1.8126	1.8126	1.6766	1.6766	1.6472	1.1879	1.1879	0.0565
1.7	1.9423	1.7839	1.7839	1.6769	1.6769	1.6459	1.2165	1.2165	0.0573
1.75	1.9403	1.7551	1.7551	1.6765	1.6764	1.6459	1.2451	1.2451	0.0604
1.8	1.9353	1.7279	1.7279	1.6751	1.6751	1.6475	1.2722	1.2722	0.0668
1.85	1.9263	1.7026	1.7026	1.6731	1.6731	1.6503	1.2974	1.2974	0.0773
1.9	1.9125	1.6792	1.6792	1.6704	1.6704	1.6541	1.3208	1.3207	0.0926
1.91	1.9096	1.6746	1.6746	1.6701	1.6701	1.6546	1.3253	1.3253	0.0959
1.92	1.906	1.6703	1.6702	1.6694	1.6695	1.6555	1.3297	1.3297	0.0998
1.93	1.9021	1.669	1.669	1.6658	1.6658	1.6561	1.334	1.3341	0.104
1.94	1.898	1.6685	1.6685	1.6615	1.6615	1.6568	1.3384	1.3383	0.1085
1.95	1.8937	1.6679	1.6679	1.6582	1.6573	1.6568	1.3426	1.3425	0.113
1.96	1.889	1.6674	1.6675	1.6583	1.6531	1.6531	1.3467	1.3467	0.1181
1.97	1.8841	1.667	1.667	1.6588	1.649	1.649	1.3508	1.3509	0.1233
1.98	1.8789	1.6664	1.6666	1.6594	1.6449	1.645	1.3549	1.3549	0.1289
1.99	1.8736	1.666	1.666	1.6601	1.641	1.6409	1.3589	1.3588	0.1346
2.0	1.868	1.6656	1.6656	1.6606	1.6371	1.637	1.3628	1.3627	0.1406

Appendix C: Sample MREOM Input File

```
      !MR-EOM DKH ma-DKH-Def2-TZVP ExtremeSCF

* xyz 1 6
Cr 0.000000 0.000000 0.000000
O  1.65 0.000000 0.000000
end

%basis
newgto Cr "ma-DKH-def2-TZVPP" end # Specifying the basis set on "Element"
newgto O "ma-DKH-def2-TZVPP" end # Specifying the basis set on "Element"
end

!MOREAD
%moinp "orca.gbw"

%casscf
nel 9
norb 9
mult 10
nroots 1
gtol 1e-12
etol 1e-12
shiftup 2
shiftdn 2
switchstep nr
end

%mdci
ewin -6, 100000
MaxIter 300
STol 1e-12
TCutInt 1e-14
Hbar_Symmetry = Vertex
LevelShift 0
DoSingularPT = True
SingularPTThresh = 0.01
End
```

```
%mrci
 ewin -6, 100000
 MaxIter 200
 citype mrci
 davidsonopt 0
 tsel 0 tpre 0 tnat 0
 Etol 1e-8 Rtol 1e-8
 RejectInvalidRefs false
 newblock 6 *
 nroots 3
 excitations none
 flags[is ] 1
 flags[sa ] 1
 flags[ia ] 0
 flags[ijss] 1
 flags[ijsa] 0
 refs cas(9,9) end
 end
 newblock 4 *
 nroots 3
 excitations none
 flags[is ] 1
 flags[sa ] 1
 flags[ia ] 0
 flags[ijss] 1
 flags[ijsa] 0
 refs cas(9,9) end
 end
 newblock 2 *
 nroots 5
 excitations none
 flags[is ] 1
 flags[sa ] 1
 flags[ia ] 0
 flags[ijss] 1
 flags[ijsa] 0
 refs cas(9,9) end
 end

 soc
 DoSOC true # include the SOC contribution
 end
end
```

Appendix D: MREOM Reference Weights and T Amplitudes per System

MnO^+

Table 15: Smallest References Weights and Largest T Amplitudes for MnO^+

Interatomic Distance (Å)	Smallest Reference Weights (High Spin)			Largest T Amplitudes (High Spin)		
1.4	0.8745	0.9036	0.9038	0.067779	0.06719	0.048935
1.45	0.8755	0.9053	0.9058	0.076563	0.060643	0.042937
1.5	0.8763	0.9066	0.9069	0.061426	0.048551	0.036614
1.55	0.8767	0.9051	0.9051	0.080213	0.077952	0.041718
1.6	0.8767	0.9033	0.9033	0.08842	0.086724	0.041006
1.65	0.8762	0.9016	0.9016	0.066612	0.06448	0.04143
1.7	0.8753	0.9	0.9	0.084372	0.045215	0.0403
1.75	0.8988	0.8988	0.9109	0.089201	0.057006	0.042703
1.8	0.8981	0.8981	0.9127	0.089327	0.084712	0.042571
1.85	0.8988	0.8999	0.9129	0.078069	0.076038	0.040513
1.95	0.9009	0.9019	0.9145	0.088258	0.086315	0.045744
2.0	0.9033	0.9041	0.9183	0.096399	0.093535	0.050526
Interatomic Distance (Å)	**Smallest Reference Weights (Low Spin)**			**Largest T Amplitudes (Low Spin)**		
1.4	0.9304	0.9304	0.9315	0.584819	0.584819	0.193995
1.45	0.9281	0.934	0.934	0.384476	0.384476	0.264742
1.5	0.9255	0.9382	0.9382	0.351814	0.237517	0.237517
1.55	0.9267	0.9424	0.9424	0.416985	0.161447	0.161447
1.6	0.9288	0.946	0.946	0.411187	0.120229	0.120229
1.65	0.9375	0.9473	0.9473	0.356044	0.095754	0.095754
1.7	0.9341	0.949	0.949	0.056244	0.054671	0.054671
1.75	0.9352	0.9487	0.9487	0.053831	0.049127	0.049127
1.8	0.9354	0.948	0.948	0.051837	0.045566	0.045566
1.85	0.9335	0.947	0.947	0.050214	0.049106	0.026308
1.9	0.9338	0.946	0.946	0.054304	0.048794	0.031118
1.95	0.9343	0.9433	0.9433	0.059901	0.047654	0.033962
2.0	0.9353	0.942	0.942	0.065933	0.046779	0.038823

FeO^+

Table 16: Smallest References Weights and Largest T Amplitudes for FeO^+

Interatomic Distance (Å)	Smallest Reference Weights (High Spin)			Largest T Amplitudes (High Spin)		
1.45	0.9251	0.9251	0.926	0.094837	0.094837	0.046668
1.5	0.9254	0.9254	0.9254	0.096946	0.096946	0.056733
1.55	0.9248	0.9249	0.9249	0.098853	0.098853	0.048946
1.6	0.9237	0.9237	0.9241	0.100491	0.100491	0.058271
1.65	0.921	0.9222	0.9222	0.101821	0.101821	0.058499
1.7	0.9198	0.9205	0.9206	0.102848	0.102848	0.042803
1.75	0.9189	0.9193	0.9193	0.103605	0.103605	0.058099
1.8	0.9184	0.9194	0.9194	0.104133	0.104133	0.057986
1.85	0.9186	0.9191	0.9191	0.104474	0.104474	0.05686
1.9	0.9181	0.9181	0.9183	0.100696	0.100696	0.053678
1.95	0.919	0.919	0.9192	0.100851	0.100851	0.053402
2.0	0.9195	0.92	0.92	0.100933	0.100933	0.045835
2.05	0.9201	0.9206	0.9206	0.100959	0.100959	0.04002
2.1	0.9211	0.9234	0.9244	0.10094	0.10094	0.047875
2.15	0.9224	0.9259	0.9266	0.100882	0.100882	0.052765
2.2	0.9241	0.9289	0.9294	0.100791	0.100791	0.052945
2.3	0.9357	0.9362	0.9363	0.100535	0.100535	0.052797
2.4	0.9429	0.9435	0.9435	0.100212	0.100212	0.051005
2.6	0.956	0.957	0.957	0.099502	0.099502	0.061972
Interatomic Distance (Å)	**Smallest Reference Weights (Low Spin)**			**Largest T Amplitudes (Low Spin)**		
1.4	0.9243	0.9267	0.9267	0.026734	0.026734	0.019473
1.45	0.9288	0.9288	0.9311	0.024898	0.024898	0.020434
1.5	0.9304	0.9304	0.9361	0.022763	0.022763	0.021764
1.55	0.9319	0.9319	0.938	0.024559	0.024559	0.02122
1.6	0.9481	0.9497	0.9551	0.02387	0.02323	0.023056
1.65	0.9452	0.9467	0.9563	0.02532	0.023763	0.020723
1.7	0.9406	0.9552	0.9572	0.027718	0.026056	0.023885
1.8	0.9516	0.9536	0.9538	0.030343	0.026321	0.023695
1.85	0.9536	0.9537	0.9567	0.031467	0.026162	0.023615
1.9	0.9548	0.9559	0.9579	0.02981	0.02981	0.025938
1.95	0.9547	0.9558	0.9583	0.028592	0.028592	0.025144
2.0	0.9545	0.9558	0.9588	0.030691	0.030691	0.023792

CoO^+

Table 17: Smallest References Weights and Largest T Amplitudes of CoO^+

Interatomic Distance (Å)	Smallest Reference Weights (High Spin)			Largest T Amplitudes (High Spin)		
1.3	0.9101	0.9101	0.9134	0.036641	0.036641	0.026966
1.35	0.9172	0.9172	0.9199	0.038946	0.038946	0.02752
1.4	0.9208	0.9209	0.9215	0.040367	0.040367	0.025495
1.45	0.9232	0.9251	0.9251	0.041698	0.041698	0.028555
1.5	0.9253	0.9278	0.9309	0.042956	0.042956	0.02558
1.55	0.9265	0.9275	0.9316	0.044075	0.044075	0.029411
1.6	0.9263	0.9269	0.9297	0.044997	0.044997	0.029458
1.65	0.9249	0.9249	0.9264	0.045731	0.045731	0.025335
1.7	0.9235	0.9235	0.9251	0.046293	0.046293	0.029166
1.75	0.9232	0.9232	0.9248	0.046707	0.046707	0.022758
1.8	0.9221	0.9221	0.9232	0.047014	0.047014	0.029217
1.85	0.9218	0.9218	0.9223	0.047264	0.047264	0.02937
1.9	0.9221	0.9222	0.9222	0.047493	0.047493	0.029556
1.95	0.923	0.9235	0.9235	0.04772	0.04772	0.029757
2	0.9234	0.9242	0.9242	0.047949	0.047949	0.029958
2.2	0.9279	0.9279	0.9305	0.048792	0.048792	0.029677
2.4	0.9479	0.9484	0.9486	0.049363	0.049363	0.030432
Interatomic Distance (Å)	**Smallest Reference Weights (Low Spin)**			**Largest T Amplitudes (Low Spin)**		
1.3	0.9374	0.9374	0.9417	0.079137	0.04656	0.026442
1.35	0.9388	0.9388	0.942	0.077046	0.040839	0.026048
1.4	0.942	0.942	0.9433	0.073187	0.036253	0.025332
1.45	0.9456	0.9456	0.9462	0.068914	0.032801	0.024545
1.5	0.9482	0.9482	0.95	0.064804	0.030311	0.024912
1.55	0.9507	0.9507	0.9517	0.061061	0.029833	0.028576
1.6	0.9524	0.9524	0.953	0.057732	0.035311	0.027407
1.65	0.9537	0.9537	0.955	0.054799	0.041268	0.026643
1.7	0.9558	0.9558	0.9567	0.052224	0.047625	0.026154
1.75	0.9549	0.9582	0.9582	0.054304	0.049957	0.02867
1.8	0.9523	0.9598	0.9599	0.061225	0.047949	0.033149
1.85	0.9489	0.9601	0.9601	0.068313	0.046152	0.038489
1.9	0.9444	0.9603	0.9603	0.075502	0.04476	0.044523
1.95	0.9388	0.9606	0.9606	0.082743	0.052035	0.043024
2.0	0.9346	0.961	0.9611	0.089869	0.060369	0.042181

NiO^+

Table 18: Smallest References Weights and Largest T Amplitudes for NiO^+

Interatomic Distance (Å)	Largest T Amplitudes (Low Spin)			Smallest Reference Weights (Low Spin)		
1.4	0.055316	0.055316	0.024297	0.945	0.945	0.9499
1.45	0.047143	0.047143	0.029071	0.95	0.95	0.9518
1.5	0.041033	0.041033	0.026089	0.9486	0.9494	0.953
1.55	0.036622	0.036622	0.02192	0.9451	0.9452	0.9531
1.6	0.033642	0.033642	0.023544	0.9431	0.9431	0.9521
1.65	0.031719	0.031719	0.022354	0.9411	0.9413	0.9508
1.7	0.030137	0.030137	0.022895	0.9398	0.9491	0.9498
1.75	0.028118	0.028118	0.023313	0.9368	0.947	0.9477
1.8	0.025557	0.025557	0.02316	0.935	0.9445	0.9454
1.85	0.0229	0.022899	0.022463	0.9414	0.9428	0.9478
1.9	0.021241	0.020565	0.020565	0.9375	0.94	0.9455
1.95	0.020077	0.020077	0.019566	0.933	0.9369	0.9404
Interatomic Distance (Å)	**Largest T Amplitudes (High Spin)**			**Smallest Reference Weights (High Spin)**		
1.45	0.102724	0.102724	0.040701	0.9188	0.9195	0.9195
1.5	0.105067	0.105067	0.046239	0.9172	0.9182	0.9182
1.55	0.106887	0.106887	0.046548	0.9161	0.9169	0.9169
1.6	0.10818	0.10818	0.036597	0.9156	0.916	0.916
1.65	0.109014	0.109014	0.043101	0.9154	0.9154	0.9159
1.7	0.109491	0.109491	0.045477	0.9152	0.9152	0.9162
1.75	0.109707	0.109707	0.045102	0.9156	0.9156	0.9165
1.8	0.109737	0.109737	0.03286	0.9163	0.9163	0.9174
1.85	0.10963	0.10963	0.044531	0.9175	0.9175	0.9191
1.9	0.109421	0.109421	0.044331	0.919	0.919	0.9198
1.95	0.109133	0.109133	0.04418	0.9207	0.9207	0.9214
2.0	0.108785	0.108785	0.044022	0.9225	0.9225	0.9231
2.05	0.108392	0.108392	0.043992	0.9236	0.9237	0.9242
2.1	0.107968	0.107968	0.043944	0.9233	0.9234	0.9242
2.15	0.107525	0.107525	0.043919	0.9231	0.9231	0.9239
2.2	0.107075	0.107075	0.045821	0.9236	0.9236	0.9238

CrO^+

Table 19: Smallest References Weights and Largest T Amplitudes for CrO^+

Interatomic Distance (Å)	Smallest Reference Weights (High Spin)			Largest T Amplitudes (High Spin)		
1.3	0.8565	0.8565	0.857	0.03607	0.03607	0.026336
1.35	0.8568	0.8568	0.8802	0.04099	0.04099	0.027402
1.4	0.8574	0.8574	0.8621	0.034482	0.034482	0.026009
1.45	0.8583	0.8583	0.8709	0.03728	0.03728	0.026184
1.5	0.8593	0.8593	0.8679	0.039295	0.039294	0.02772
1.55	0.8605	0.8605	0.8665	0.042795	0.042794	0.029141
1.6	0.862	0.862	0.8665	0.04395	0.04395	0.029748
1.65	0.8637	0.8637	0.8677	0.045261	0.045261	0.03071
1.675	0.8647	0.8647	0.8686	0.045731	0.04573	0.030853
1.7	0.8658	0.8658	0.8699	0.04501	0.044697	0.029854
1.75	0.8684	0.8684	0.873	0.045342	0.045337	0.03353
1.8	0.8716	0.8716	0.8769	0.045586	0.045583	0.039762
1.85	0.8753	0.8753	0.8814	0.04707	0.047057	0.044981
1.9	0.8794	0.8794	0.8861	0.055737	0.05573	0.044079
1.95	0.884	0.884	0.8909	0.066046	0.066042	0.043321
2.0	0.8886	0.8886	0.8954	0.078296	0.078286	0.046241
2.1	0.8972	0.8972	0.9026	0.109637	0.109594	0.053148
2.2	0.9035	0.9035	0.9073	0.150908	0.150875	0.065657
2.4	0.9096	0.9096	0.9109	0.24328	0.243191	0.106005
Interatomic Distance (Å)	**Smallest Reference Weights (Low Spin)**			**Largest T Amplitudes (Low Spin)**		
1.4	0.9492	0.9498	0.9502	0.031713	0.031708	0.025191
1.45	0.9506	0.9515	0.9572	0.028477	0.028477	0.024575
1.5	0.9512	0.9515	0.9605	0.061238	0.057134	0.023584
1.55	0.9536	0.9556	0.9592	0.212437	0.208189	0.043411
1.6	0.9524	0.9536	0.9604	0.047928	0.047923	0.047856
1.65	0.9517	0.953	0.9598	0.129287	0.129279	0.129276
1.7	0.9497	0.9526	0.9613	0.070278	0.070278	0.070277
1.75	0.9454	0.9505	0.9603	0.034229	0.034229	0.034229
1.8	0.9358	0.9467	0.9583	0.021992	0.021495	0.021495
1.95	0.9157	0.9447	0.9506	0.02479	0.02479	0.024088
2.0	0.9158	0.9464	0.9489	0.026011	0.026011	0.025764